FEASIBILITY OF A NEW TECHNIQUE TO DETERMINE DYNAMIC TENSILE BEHAVIOR OF BRITTLE MATERIALS

Andrew W. Dean

Thesis Prepared for the Degree of

MASTER OF SCIENCE

UNIVERSITY OF NORTH TEXAS

May 2016

APPROVED:

Weihuan Zhao, Major Professor
Xu Nie, Co-Advisor, Committee Member
Xiaohua Li, Committee Member
Cherish Qualls, Committee Member
Yong Tao, Department Chair
Tae-Youl Choi, Graduate Advisor
Costas Tsatsoulis, Dean of Toulouse Graduate School

Dean, Andrew W. *Feasibility of a New Technique to Determine Dynamic Tensile Behavior of Brittle Materials.* Master of Science (Mechanical and Energy Engineering), May 2016, 66 pp., 52 figures, references, 6 titles.

Dynamic tensile characterization of geo-materials is critical to the modeling and design of protective structures that are often made of concrete. One of the most commonly used techniques currently associated with this type of testing is performed with a Kolsky bar and is known as the spall technique. The validity of the data from the spall technique is highly debated because the necessary boundary conditions for the experiment are not satisfied. By using a technique called pulse shaping, a new "controlled" spall technique was developed to satisfy all boundary conditions so that the analyzed data may be useful in modeling and design. The results from this project were promising and show the potential to revolutionize the way Kolsky bar testing is performed.

ACKNOWLEDGEMENTS

First and foremost I would like to thank my advisor Dr. Xu Nie. Dr. Nie was a fantastic mentor who introduced me to the world of the dynamic behavior of materials. Dr. Nie helped arranged my internship with the Air Force and guided me each step of the way. He offered autonomy in the lab while always being available, understanding and quick to respond.

Thank you to the Air Force Research Lab, and in particular Dr. Bradley Martin, for the internship opportunity at the research facility in Florida, as well as much of the funding. It was under the excellent guidance of Dr. Martin that I was able to perform much of the experimental work for this thesis. Additionally, Koby Kennison worked at the Air Force Lab and was instrumental in working with the DIC equipment.

Thank you to the Army Engineer Research and Development Center, and in particular Dr. William Heard, who was the primary party of interest in this project, as well as much of the funding. Dr. Heard and his team, in particular Brett Williams, provided all the core samples needed for this project and drove them to Florida to be used.

Thank you to the University of North Texas and, in particular, my committee members Dr. Weihuan Zhao, Dr. Xiaohua Li and Dr. Cherish Qualls for all the expert guidance, use of facilities and opportunities made available during my academic years.

TABLE OF CONTENTS

ACKNOWLEDGEMENTS iii
LIST OF FIGURES vi
NOMENCLATURE viii
INTRODUCTION 1
Background 1
Pulse Shaping 3
Laser Extensometer 3
DIC 4
Problem Statement 4
Spall Technique 4
Thesis Overview 5
LITERATURE REVIEW/THEORY 7
Split Hopkinson (Kolsky) Bar Design, Testing and Application [1] 7
A New Theory for Kolsky Bar Dynamic Spall Tests [6] 16
The Spalling of Long Bars as a Reliable Method [5] 20
About the Dynamic Uniaxial Tensile Strength of Concrete-Like Materials [4] 20
EXPERIMENTAL SETUP 22
Modified Kolsky Bar 22
Specimens 27
Shield 28
Momentum Trap 28
Pulse Shapers 29
Laser Extensometer 30
RESULTS, ANALYSIS AND DISCUSSION 40
Initial Conditions 40
Determining the Spall Strength 44
Determining Strain Rate 54
CONCLUSION 60
Future Work 61
APPENDIX A: MATLAB CODE FOR BATCH PROCESSING 62

APPENDIX B: ADAPTER CAD DRAWING 65
REFERENCES 66

LIST OF FIGURES

Figure 1.1 Compression Bar 2
Figure 1.2 Spall Setup 5
Figure 2.1 Tank, Barrel and Firing Assembly at UNT 8
Figure 2.2 Linear bearings supporting a Kolsky bar 9
Figure 2.3 Strain Gages shown mounted on an incident Bar 9
Figure 2.4 Image of a Wheatstone bridge 10
Figure 2.5 Stress waves in bars 12
Figure 2.6 Modified momentum trap 14
Figure 2.7 A Kolsky bar setup using a laser to track displacement 15
Figure 2.8 Stress wave reflection and overlap in a spall specimen 19
Figure 2.9 Schematic illustrating how to create a uniform tensile stress in the spall specimen through the interaction of two isosceles triangular waves 20
Figure 3.1 Barrel mounting and firing setup 23
Figure 3.2 Striker with attached sabots 23
Figure 3.3 Linear bearings, mounting blocks and shims 24
Figure 3.4 Striker aligned with incident bar 25
Figure 3.5 Firing assembly 25
Figure 3.6 Momentum trap with incident bar (and attached flange) protruding 26
Figure 3.7 Strain gages attached to incident bar 27
Figure 3.8 Specimen holders with translation stages and custom adapters 28
Figure 3.1 Spall setup showing momentum trap 29
Figure 3.2 Fan beam laser directed into lens 30
Figure 3.3 Schematic showing top and side views of laser optics 31
Figure 3.4 Specimen calibration model on translation stage 32
Figure 3.5 Laser setup 33
Figure 3.6 Graph showing laser sensitivity (slope) 33
Figure 3.7 Makeshift box covering laser setup 34
Figure 3.8 Camera and LED light setup 35
Figure 3.9 Laser signal setup 36
Figure 3.10 DIC setup showing cameras, flashes and software 37

Figure 3.11 Correlated Solutions calibration substrate 38
Figure 3.12 Speckled specimen with superimposed strain calculation 39
Figure 4.1 Wave form showing slope comparison from UNT 42
Figure 4.2 Wave form with slope comparison from UF-REEF 42
Figure 4.3 Comparison of wave forms to illustrate repeatability 43
Figure 4.4 Alignment between incident bar and glass sample 45
Figure 4.5 Strain plus displacement in glass specimen 45
Figure 4.6 Glass sample showing failure during event 46
Figure 4.7 Figure showing (a) tensile failure striations and (b) random failure 46
Figure 4.8 Figure showing (a) specimen failure in compression and (b) specimen failure in tension 47
Figure 4.9 Valid sample with cracks identified 48
Figure 4.10 Specimen displacement from laser data 49
Figure 4.11 Velocity of specimen derived from displacement 49
Figure 4.12 Specimen velocity shown with filter applied 50
Figure 4.13 Filtered velocity/time data of specimen 50
Figure 4.14 Velocity deviation point indicating spall 51
Figure 4.15 DIC software analysis of specimen 54
Figure 4.16 Graph of raw data showing incident and reflected waves 55
Figure 4.17 Stress transmitted into sample 56
Figure 4.18 Strain rate profile of specimen 57
Figure 4.19 Summation of compression and reflected waves now in tension 58

NOMENCLATURE

Abbreviations

UNT = University of North Texas

UF-REEF = University of Florida Research and Engineering Education Facility

DIC = Digital Image Correlation

AFRL = Air Force Research Lab

ERDC = Army Engineer Research and Development Center

Greek Letters

ε = strain

U_0 = voltage output

U_I = excitation voltage

G_a = gain

G_F = gage factor

$\sigma_I =$ internal stress

ρ = density

ρ_B = density of the bar

C_B = wave speed of the bar

C_w = wave speed in specimen

v_{st} = velocity of striker

Δt = change in time

l_B = length of bar

E = modulus of elasticity

R^2 = curve fitting parameter

L_S = laser sensitivity

CHAPTER 1

INTRODUCTION

Dynamic tensile characterization of geo-materials is critical to the modeling and design of protective structures that are often made of concrete. One of the most commonly used techniques currently associated with this type of testing is known as the spall technique. The validity of the data from the spall technique is highly debated because the necessary boundary conditions for the experiment are not satisfied. The objective of this project is to develop a controlled spall technique that satisfies all boundary conditions so that the analyzed data may be useful in modeling and design.

Background

Typically, compression and tensile properties of materials are measured using "quasi-static" testing. Quasi-static testing machines are capable of subjecting samples to large forces (100-600 kN) at speeds of less than 0.01 m/s. This means that conventional material testing is performed at low strain rates (less than 10 (s^{-1})). Using quasi-static testing, a material is deformed so slowly that its material properties are analogous to static loading.

When modeling systems with high-speed impact (i.e. vehicle crashes, flying debris, aerospace products etc.), engineers need data that accurately describes how materials behave under impact conditions. This is necessary because the mechanical properties of many materials (in particular, brittle materials) can vary greatly when subjected to high-strain rate loadings (on the order of 10^2 to 10^4 (s^{-1})).

Measuring the material's mechanical response under impact loading creates a challenge not present in quasi-static tests. Quasi –static machines use a closed-loop feedback system to monitor and control testing conditions. Since high strain rates are beyond the scope of quasi-static machines, a direct impact open-loop system is the alternative. Using this setup for impact loading, however, creates two major issues. First, during a direct impact with a specimen, little information can be recorded. Second, the loading conditions on the specimen are not well controlled.

In 1949 Herbert Kolsky devised a clever method of measuring a material's response to impact loading. Instead of directly impacting on the specimen, he placed two elastic rods on both sides of the specimen and then struck one of the rods [1]. The bar between the striker and the specimen is known as the incident bar and the other bar is called the transmission bar (see Figure 1.1). Using this arrangement "the impact event is controllable and quantitative" [1] because the impact force can be precisely measured as it travels along the bars in the form of a stress wave.

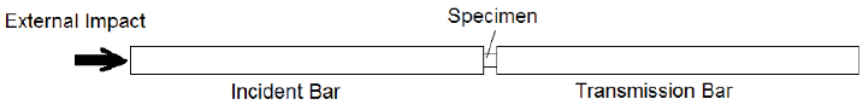

Figure 0.1 Compression Bar

Since Kolsky invented this technique, researchers have been continuously working to improve the accuracy of Kolsky Bar experiments and adapting their techniques to test samples under a variety of impact loading conditions including compression, tension, torsion, and even triaxial loadings. One of those iterations is the spall technique.

Pulse Shaping

Unlike conventional low strain-rate material testing machines (i.e. quasi-static machines), the Kolsky bar technique does not have a feedback control mechanism to actively monitor the boundary conditions (stress equilibrium and strain rate) as the specimen is being deformed. The open feedback loop requires the boundary conditions to be controlled by the initial loading wave. Controlling the initial loading wave is achieved by designing the loading wave profile through the use of the pulse shaping technique, and is monitored by the use of an oscilloscope. The pulse shaping technique involves placing a relatively soft material, or "pulse shaper" on the impact end of the incident bar. When the striker impacts the incident bar it plastically deforms the soft pulse shaper material which alters the shape of the incident wave [1]. By changing the pulse shaper material, geometry, and striking velocity, the incident wave profile can be precisely tailored.

Obtaining the spall velocity of the specimen as it fails is necessary to accurately analyze the data. Two methods are being explored to measure this velocity: a laser extensometer and high-speed photography.

Laser Extensometer

A laser extensometer consists of a flat laser beam that is projected into a light sensor. When the specimen spalls, the spalled end will move past the laser sensor blocking the laser and reducing the amount of light seen by the sensor. The reduction of light is recorded and used to calculate the displacement of the spalled piece during the event. The displacement history is used to calculate the velocity by performing a single time derivative.

DIC

The second measurement method involves using high speed cameras and is called Digital Image Correlation (DIC). In the DIC technique, the specimen is painted with a speckled pattern. Two (offset) cameras focused on the speckle pattern are then synchronized to each other for 3-D DIC analysis. Based on the acquired high-speed images the DIC software tracks the displacement of the speckles painted on the specimen. DIC measures the displacement history on the specimen surface from which velocity and strain can be calculated.

Problem Statement

Using the current dynamic mechanical characterization technique, the validity of constitutive properties for concrete, specifically the dynamic tensile data, is highly controversial due to the experimental conditions not being well defined.

Spall Technique

The spall technique is set up using what is known as a modified Kolsky Bar. In this setup, a striker impacts the incident bar sending a stress wave down the incident bar into a specimen (see Figure 1.2). A transmission bar is not used, so after the stress wave travels through the specimen to the free end, it is reflected back as a tensile load. Since brittle materials are inherently weaker in tension than in compression, the experiment can be designed in a way to ensure that the sample fails (or spalls) under the tensile load.

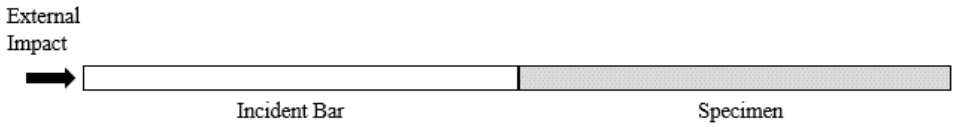

Figure 0.2 Spall Setup

Constant strain rate and uniform stress in the sample are necessary to validate any compression or tension testing technique [1]. Using the traditional spall technique, both stress and strain rate vary significantly along the length of the specimen. These variations do not satisfy the boundary conditions and are the source of many debates over the validity of the experimental results. For this project the traditional spall technique has been modified. Through certain modifications to the loading wave, accurate control of the strain rate and stress distribution within the specimen becomes possible. The new technique is called the "controlled spall technique", and the modifications were made using pulse shaping.

Thesis Overview

It is well established in solid mechanics literature that the failure strength of concrete and other brittle geo-materials are often highly rate dependent. Many studies have reported that the failure strength of concrete can be as much as 2 or 3 times higher when deformed at high strain rates [2]. In order to obtain accurate experimental data on the failure of concrete at high rates, the specimens must be deformed at a known constant strain-rate and under uniform stress state [1]. The focus of this thesis is to use a combination of two methods to verify the validity of the "controlled spall technique". The pulse shaping technique is used to satisfy loading boundary conditions, while the spall technique is the basis technique (with the above mentioned modification). If shown to be feasible, the new technique will satisfy the boundary conditions

required to yield well defined, accurate results for determining the dynamic tensile strength of brittle materials.

CHAPTER 2

LITERATURE REVIEW/THEORY

Split Hopkinson (Kolsky) Bar Design, Testing and Application [1]

"Split Hopkinson (Kolsky) Bar Design, Testing and Application" does not directly address the spall technique. It does, however, lay much of the theory and groundwork that the spall technique uses by discussing the Kolsky compression bar. The Kolsky compression bar uses many of the same principles and basic functions as the spall technique, which will be the focus of this review.

Setup

The three basic components of a Kolsky Bar system include: a loading device, bar components and a data acquisition system.

1) Loading Device

   The most common loading system consists of a gas gun that fires a striker. This provides efficient, controllable and repeatable impact momentum.

   The gas gun is made up of a pressure vessel, a gun barrel, a valve assembly and a striker (see Fig 2.1). The pressure vessel is pre-loaded with compressed air or gas to a predetermined pressure. The valve is used to promptly release that air from its reservoir into the gun barrel within which a striker is propelled. Gas venting holes are drilled along the sides of the gun barrel near the exit to bleed the excessive pressure before impact. The striker speed is changed by varying the pressure in the pressure vessel or by changing the

acceleration distance. The loading duration on the incident bar generated by the impact is directly proportional to the length of the striker.

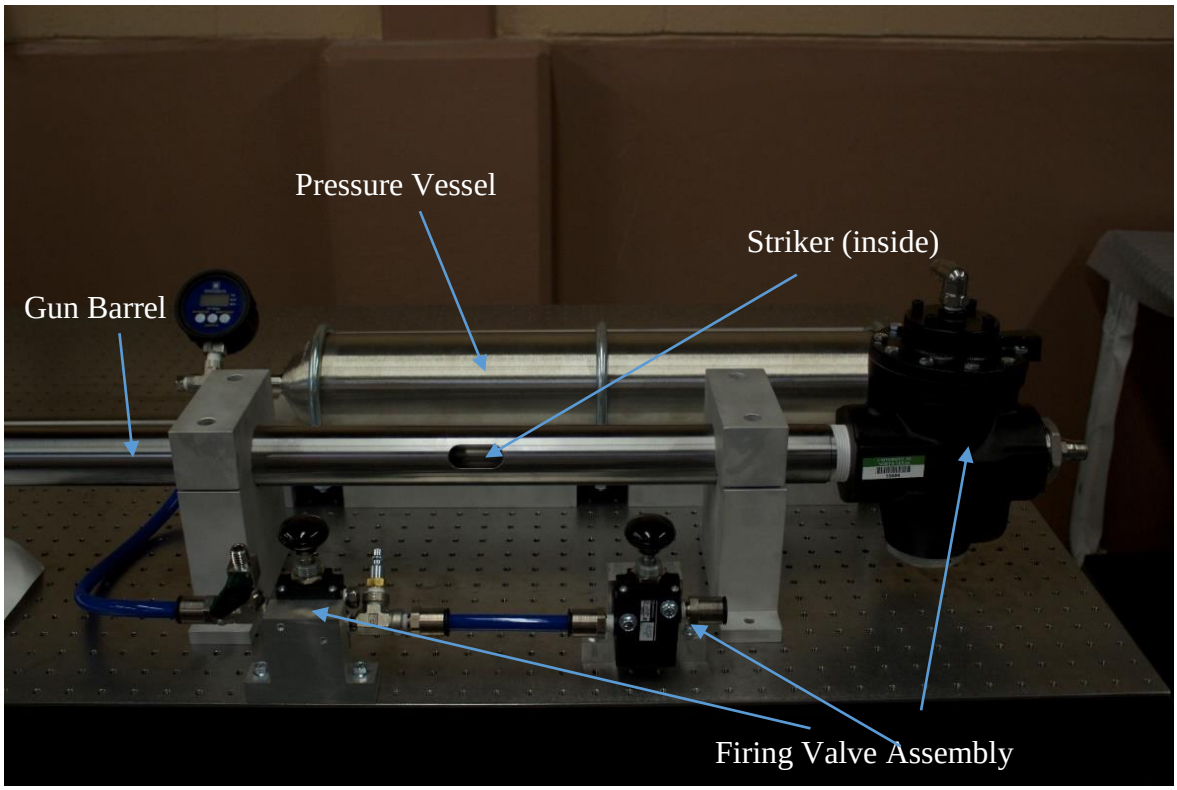

Figure 0.1 Tank, Barrel and Firing Assembly at UNT

2) Bar Components

For this review, the bar components section will focus only on the incident bar. The incident bar is, ideally, the same diameter as the striker. The bars (striker and incident) are made of the same material (C300 Maraging steel). Stress waves traveling inside the incident bar are measured using strain gauges mounted on the surface of the incident bar. Since surface strains are used to measure internal stress, the stress wave in the bar has to remain one dimensional. Also the bars must be perfectly aligned and

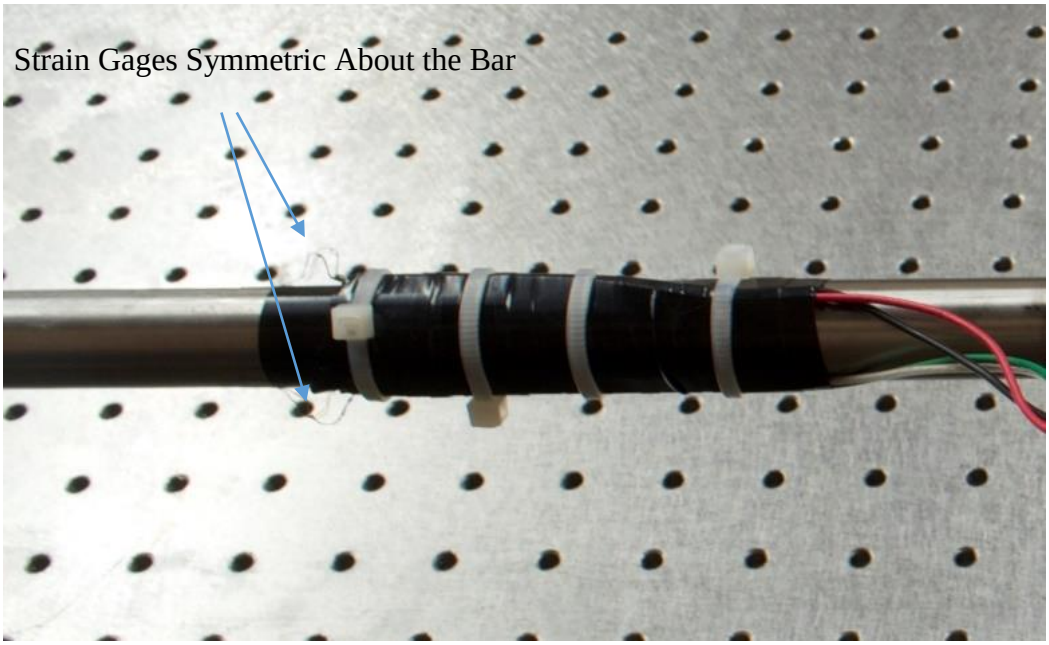

Figure 0.3 Strain Gages shown mounted on an incident Bar

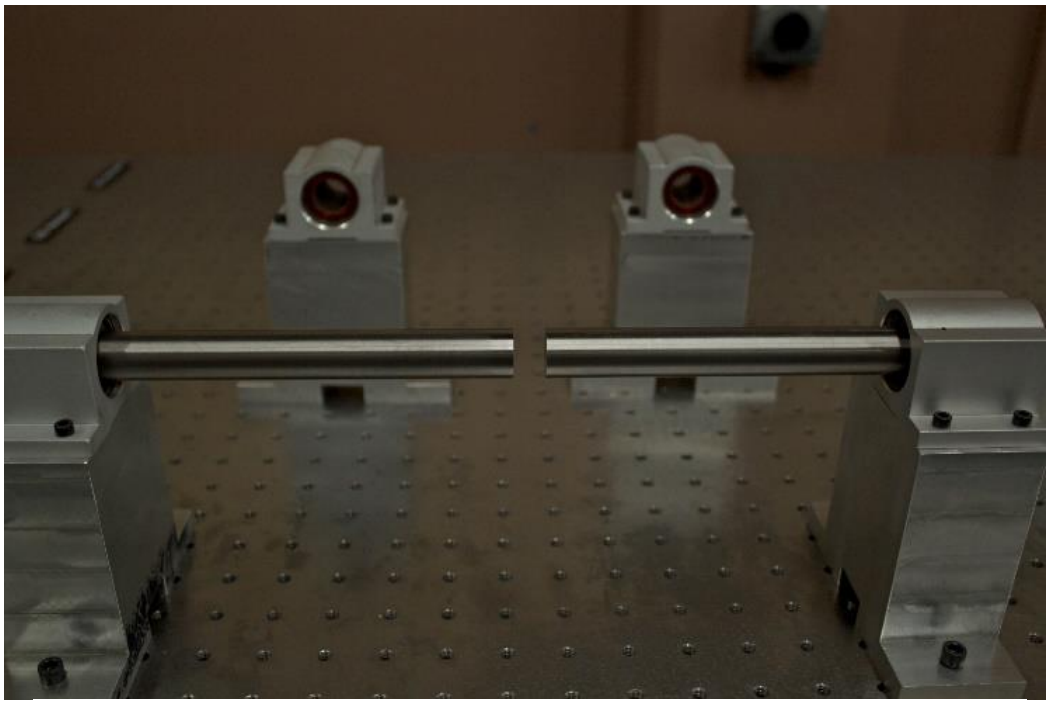

Figure 0.2 Linear bearings supporting a Kolsky bar

straight along the loading axis so that no bending or shear is introduced during the striker impact. The incident bar must be allowed to move axially with minimum friction. This is

achieved using high precision, well lubricated linear bearings (see Fig 2.2). Also, the incident bar must be at least twice as long as the striker to avoid overlap between the incident and reflected pulses.

3) Data Acquisition System

Two strain gauges are attached on the incident bar, symmetrically across the bar diameter (see Fig 2.3). The voltages produced from the strain gauges are conditioned with a Wheatstone bridge and then amplified. For this project, two Wheatstone bridges were constructed, one for use at UNT and one for the UF-REEF (see Fig 2.4).

Figure 0.4 Image of a Wheatstone bridge

An image of the wave is displayed on an oscilloscope. It was determined that for a half bridge configuration, the relationship between strain (ε), output voltage(U_0), excitation voltage (U_I), gain (G_a) and gage factor (G_F) is:

$$\varepsilon = \frac{2*U_0}{G_F*U_I} \tag{2.1}$$

Calibration and Data Reduction

One simple way to verify the alignment of the striker and incident bar is to fire the striker with no pulse shapers. The pulse that results from the impact should reveal a predictable rectangular shape (see Fig 2.5 a). A misaligned system will distort the pulse baseline (see Fig 2.5 b).

If the velocity is known, the stress and strain may be calculated by:

$$\sigma_I = \frac{1}{2}\rho_B C_B v_{st} \tag{2.2}$$

And

$$\varepsilon_I = \frac{1}{2} * \frac{v_{st}}{C_B} \tag{2.3}$$

The wave speed in the bar may be determined by:

$$C_B = \frac{2l_B}{\Delta t} \tag{2.4}$$

The wave velocity of the bar (or specimen) may be determined by:

$$C_w = \sqrt{\frac{E}{\rho}} \tag{2.5}$$

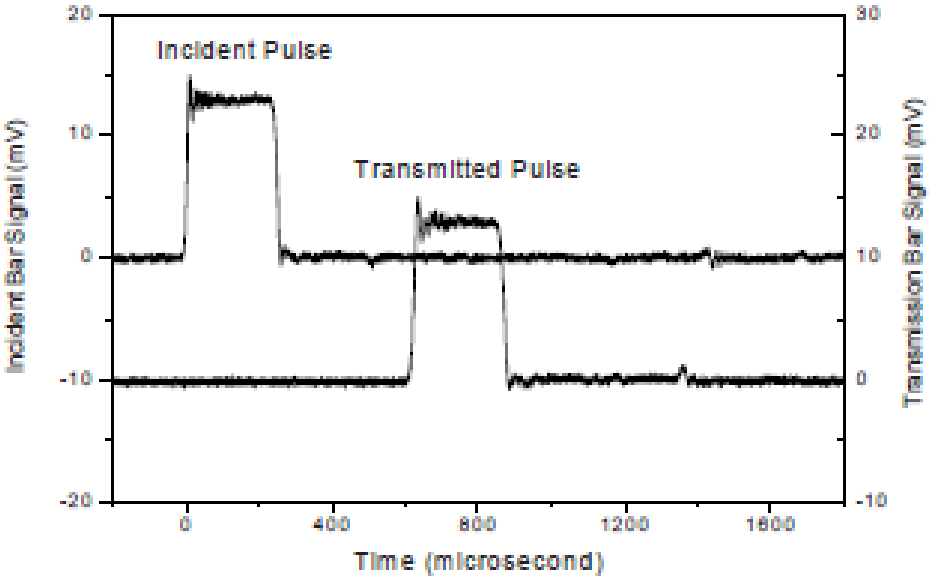

(a)

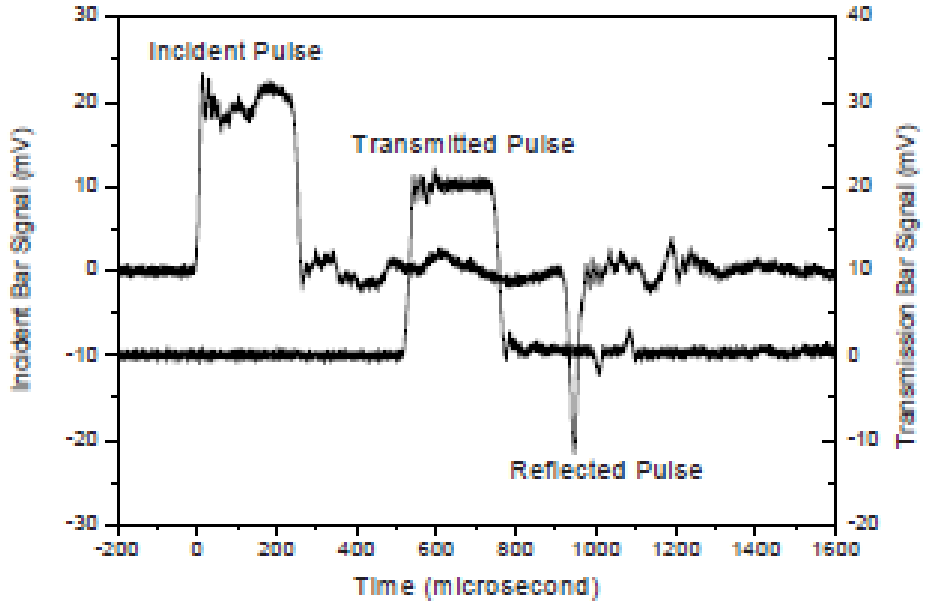

(b)

Figure 0.5 Stress waves in bars
(a) in good alignment and (b) misaligned
(Reproduced from Chen [3] with permission)

Testing Conditions

When characterizing material properties on Kolsky bars, it is necessary for the specimen to deform uniformly under well-controlled testing conditions in order for the results to be clearly interpreted and documented. With a Kolsky bar setup, feedback control mechanisms are not available which makes it challenging to subject the specimen to the specified loading conditions.

Wave Dispersion

Due to Poisson's effect, the bar material being "pushed" forward by a compressive wave is also pushed outward in the radial direction. This causes inertia-induced stress in the bar. The combination of these two effects is called wave dispersion. It was determined that with the use of a pulse shaper, corrections for wave dispersion were not necessary, and the effects of the wave dispersion were minimized to below the detectable level.

Constant Strain Rate Deformation

The Kolsky bar is designed to obtain families of stress-strain curves as a function of strain rate for the material under investigation. Therefore, it is desired for the strain rate for each stress strain curve to be constant. Constant strain rate is of particular importance in strain-rate sensitive materials. Typically, the traditional rectangular pulse does not satisfy the requirement of constant strain rate.

Pulse Shaping

Pulse shaping is used to facilitate stress equilibrium and constant strain rate in the specimen through properly modifying the profile of the incident pulse based on the material's response in a standard Kolsky bar experiment. As mentioned above, it was determined that pulse shaping also minimized the effects of wave dispersion.

Single Loading Control

When a striker impacts the incident bar, the resulting stress wave propagates within the bar. In order to control the wave reverberation in the system, Song and Chen [2] modified a momentum trap (a large rigid mass designed to stop the forward momentum of the incident bar by blocking a flange that is threaded to the impact end of the incident bar) concept and developed a single loading device (see Fig 2.6). This new design was determined not to affect the application of the pulse shaping technique.

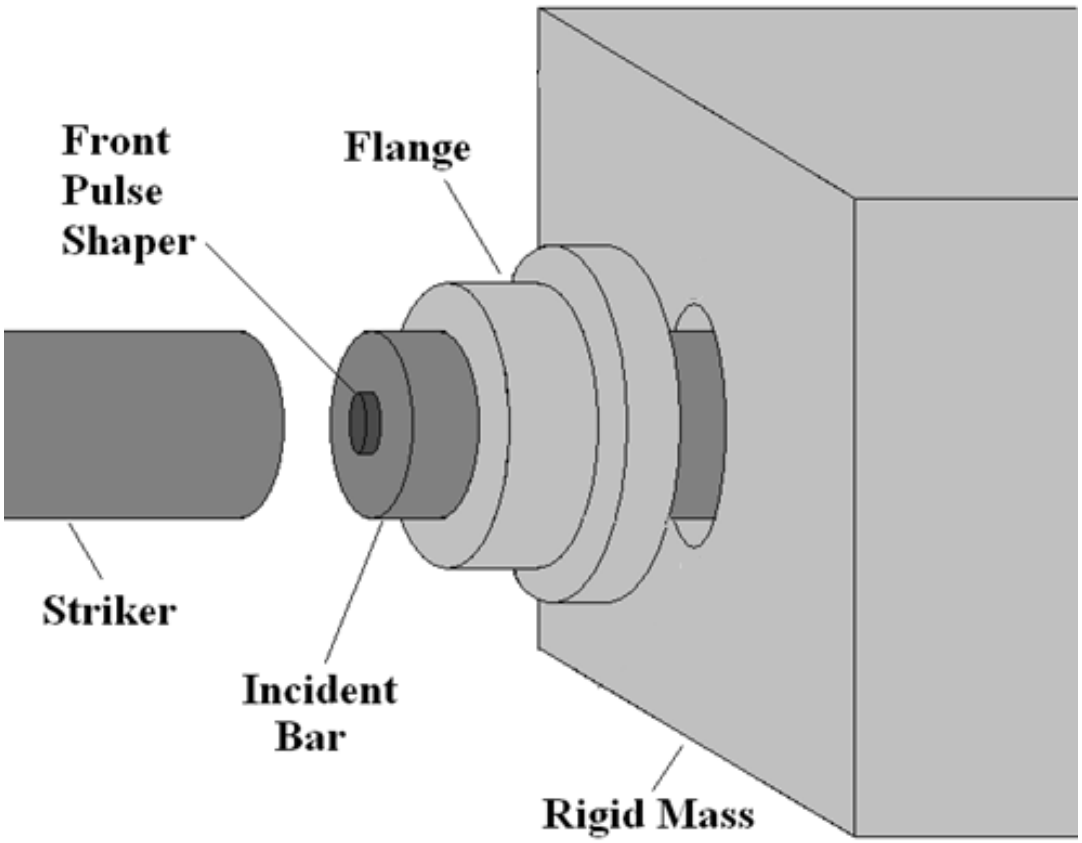

Figure 0.6 Modified momentum trap
(Reproduced from Song and Chen [2] with permission)

Laser Extensometer

In one example, Cheng [3] used a laser displacement measurement device to measure the actual strain history in the specimen. This setup consists of a laser diode, a line head and a photo detector. In this setup, the laser was used to measure the change in gap size by recording the displacement history of the gap with the photo detector (see Fig 2.7).

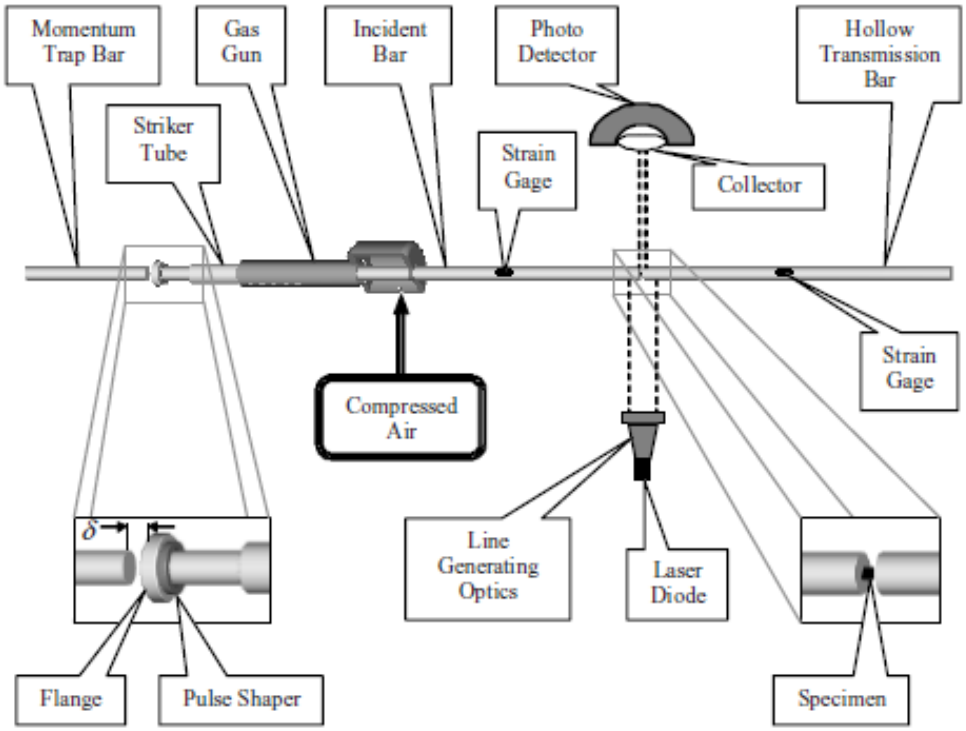

Figure 0.7 A Kolsky bar setup using a laser to track displacement

Digital Image Correlation (DIC)

Digital image correlation (DIC) is a non-contact measurement technique. In this technique a random or regular pattern with high contrast is applied to the specimen surface. High speed digital cameras are calibrated/synchronized to each other so that two images from different

angles are projected to the aperture of one camera. The images track the consecutive changes of the pattern when the specimen is subject to high speed deformation. The patterns are correlated to yield a 3-D full field deformation in the specimen. More comprehensive information of the distribution of strain over the entire specimen is obtained.

A New Theory for Kolsky Bar Dynamic Spall Tests [6]

This publication shows the theoretical proof supporting the experiments performed for this thesis. Specifically, this publication addresses the satisfaction of the boundary conditions by the modification of the stress wave profile.

Analysis:

Tensile stress in a spall specimen is generated when the incident compressive wave reflects back at the free surface of the specimen as a tensile wave. The resulting tensile stress profile in the specimen, however, is determined by the overlap between both the incident and reflected waves. Figure 2.8 presents a general schematic of wave reflection/overlap in a spall specimen with a linear elastic material response. The left-travelling reflected tensile stress wave $\sigma_1 = g(x,t)$ has the same profile and amplitude as the right-travelling incident compressive wave $\sigma_2 = f(x,t)$. At any location x_0 within the region where $f(x,t)$ and $g(x,t)$ overlap with each other, the stress in the specimen is given by:

$$\sigma(x_0,t) = f(x_0,t) + g(x_0,t) \tag{2.6}$$

While the stresses at two neighboring locations, $x_0 + \Delta x$ and $x_0 - \Delta x$, are:

$$\sigma(x_0 + \Delta x,t) = f(x_0 + \Delta x,t) + g(x_0 + \Delta x,t) \tag{2.7}$$

$$\sigma(x_0 - \Delta x, t) = f(x_0 - \Delta x, t) + g(x_0 - \Delta x, t) \quad (2.8)$$

The strain rate at location x_0, for any given time instance *t*, is defined by:

$$\partial\varepsilon(x_0, t)/\partial t = (\partial g(x_0, t)/\partial t + \partial f(x_0, t)/\partial t)/E \quad (2.9)$$

where *E* is the Young's modulus of the specimen. The strain rates at $x_0 + \Delta x$ and $x_0 - \Delta x$ are:

$$\partial\varepsilon(x_0 + \Delta x, t)/\partial t = (\partial g(x_0 + \Delta x, t)/\partial t + \partial f(x_0 + \Delta x, t)/\partial t)/E \quad (2.10)$$

$$\partial\varepsilon(x_0 - \Delta x, t)/\partial t = (\partial g(x_0 - \Delta x, t)/\partial t + \partial f(x_0 - \Delta x, t)/\partial t)/E \quad (2.11)$$

Similarly, the strain rate of location x_0 at time instances $t + \Delta t$ and $t - \Delta t$ are:

$$\partial\varepsilon(x_0, t + \Delta t)/\partial t = (\partial g(x_0, t + \Delta t)/\partial t + \partial f(x_0, t + \Delta t)/\partial t)/E \quad (2.12)$$

$$\partial\varepsilon(x_0, t - \Delta t)/\partial t = (\partial g(x_0, t - \Delta t)/\partial t + \partial f(x_0, t - \Delta t)/\partial t)/E \quad (2.13)$$

Considering the respective travelling directions of the incident and reflective waves, and assume $|\Delta x| = C_0\Delta t$ (C_0 is the one dimension wave speed in the spall specimen), Eqs. (2.12) and (2.13) can be rewritten as:

$$\partial\varepsilon(x_0, t + \Delta t)/\partial t = (\partial g(x_0 + \Delta x, t)/\partial t + \partial f(x_0 - \Delta x, t)/\partial t)/E \quad (2.14)$$

$$\partial\varepsilon(x_0, t - \Delta t)/\partial t = (\partial g(x_0 - \Delta x, t)/\partial t + \partial f(x_0 + \Delta x, t)/\partial t)/E \quad (2.15)$$

To satisfy the constant strain rate deformation criterion, the strain rate in the spall specimen should be independent of either location (*x*) or time (*t*). Therefore the following relation has to hold:

$$\partial\varepsilon(x_0 + \Delta x, t)/\partial t = \partial\varepsilon(x_0 - \Delta x, t)/\partial t = \partial\varepsilon(x_0, t + \Delta t)/\partial t = \partial\varepsilon(x_0, t - \Delta t)/\partial t \quad (2.16)$$

Using Eqs. (2.10), (2.11), (2.14), (2.15) in light of Eq. (2.16) yields:

$$\partial g(x_0 + \Delta x, t)/\partial t = \partial g(x_0 - \Delta x, t)/\partial t \quad (2.17)$$

$$\partial f(x_0 + \Delta x, t)/\partial t = \partial f(x_0 - \Delta x, t)/\partial t \quad (2.18)$$

The only solution for Eqs. (2.17) and (2.18) under any given x_0 and Δx are $\partial g(x,t)/\partial t = C_1,\ \partial f(x,t)/\partial t = C_2$, where C_1 and C_2 are constants. This solution indicates that within the section of the specimen where the incident and reflected waves interact, both waveforms have to present linear stress profiles to maintain constant strain rate deformation. Under this condition, Eqs. (2.7) and (2.8) can be re-written as:

$$\sigma(x_0 + \Delta x, t) = f(x_0, t) - C_2\Delta t + g(x_0, t) + C_1\Delta t \quad (2.19)$$

$$\sigma(x_0 - \Delta x, t) = f(x_0, t) + C_2\Delta t + g(x_0, t) - C_1\Delta t \quad (2.20)$$

If the specimen is under uniform stress state, then:

$$\sigma(x_0 + \Delta x, t) = \sigma(x_0 - \Delta x, t) \quad (2.21)$$

Substituting Eqs. (2.19) and (2.20) into Eq.(2.21) leads to $C_1 = C_2$. Note that C_1 and C_2 are the first order derivatives in time domain ($\sigma - t$). To relate them to the stress slopes in the space domain ($\sigma - x$) as shown in Fig. 2.8, one has to take into account that $g(x,t)$ is a left-travelling wave while $f(x,t)$ is a right-travelling wave. Therefore the following relation has to stand within the region of wave interaction where constant strain rate is maintained:

$$\partial g(x,t)/\partial x = -\partial f(x,t)/\partial x \quad (2.22)$$

The above analysis has shown that maintaining constant strain rate deformation and uniform stress in a spall specimen is theoretically possible if a portion of the incident and reflected waves carry a linear stress profile with opposite slopes in space domain. Considering that the reflected wave is actually the tensile version of the incident wave in

Kolsky bar spall experiments, the incident wave itself essentially needs to carry the two linear stress profiles with opposite slopes. A possible experimental solution satisfying this requirement is to design an incident stress wave that resembles an isosceles triangle, as illustrated in Fig. 2.9. For this particular waveform, when the rising edge of the reflected wave fully enters the spall specimen and interacts with the trailing edge of the incident wave, a region with uniform tensile stress is generated (area between the dotted lines). As both waves propagate through the specimen the amplitude of the uniform tensile stress increases until the brittle specimen fractures. Note that the isosceles incident waveform is a special case of the solutions for Eqs. (2.17) and (2.18), therefore the constant strain rate criterion is automatically satisfied.

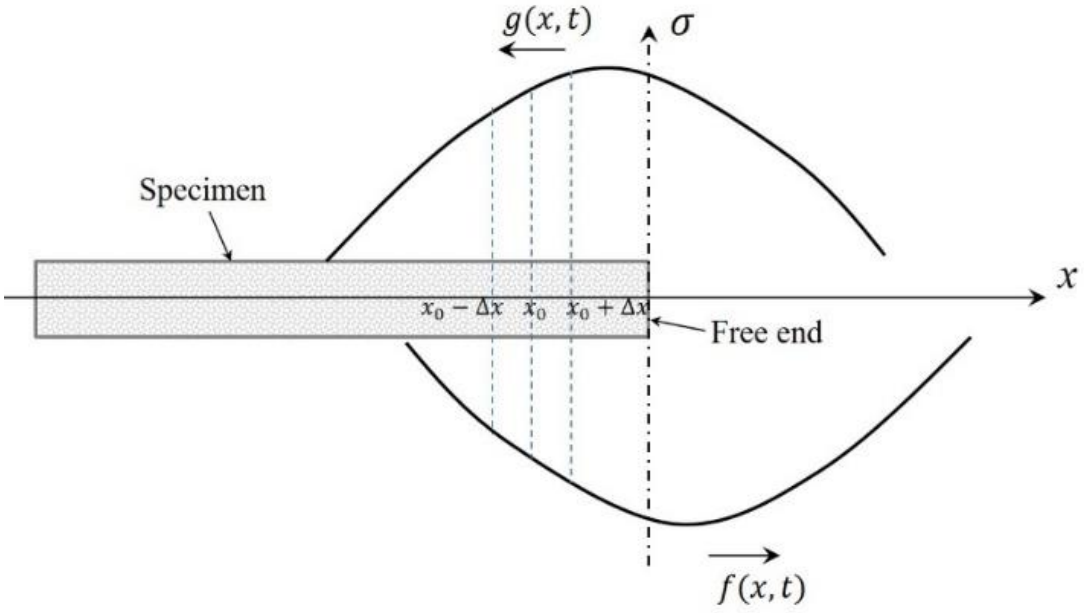

Figure 0.8 Stress wave reflection and overlap in a spall specimen

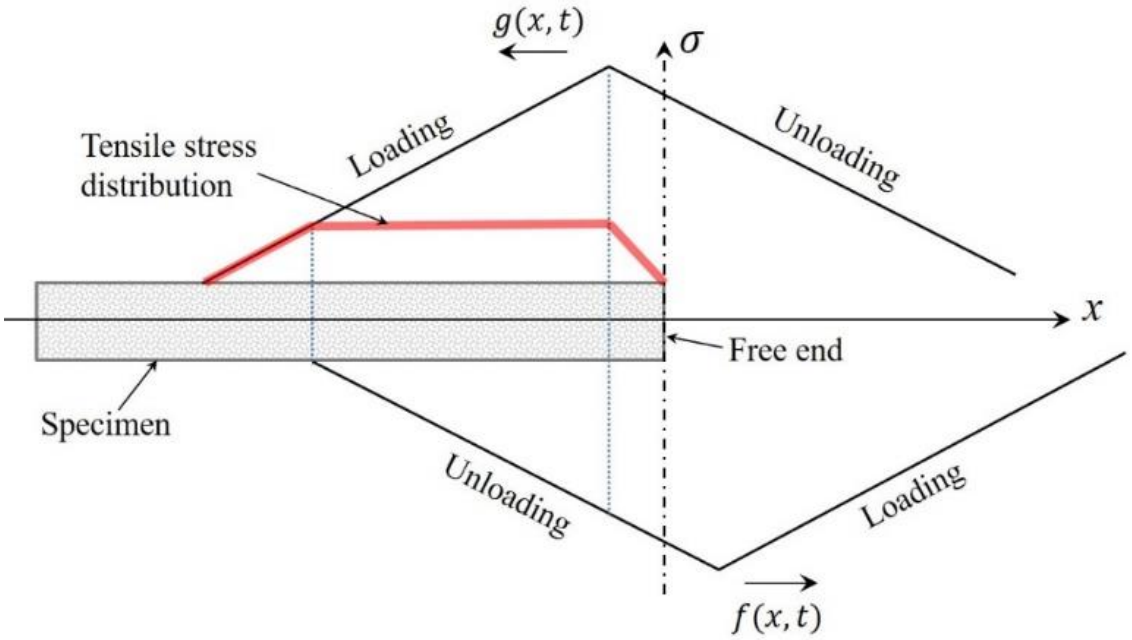

Figure 0.9 Schematic illustrating how to create a uniform tensile stress in the spall specimen through the interaction of two isosceles triangular waves

The Spalling of Long Bars as a Reliable Method [5]

Here the author discusses the difficulties of achieving stress equilibrium in the specimen as well as the general setup of the spall technique. The author used strain gages and high speed cameras to determine the spall strength and strain rate using a newly proposed method. The author's proposed method of determining the spall strength from the reflected pulse of the spall event showed questionable results.

About the Dynamic Uniaxial Tensile Strength of Concrete-Like Materials [4]

"About the Dynamic Uniaxial Tensile Strength of Concrete-Like Materials" discussed and compared several different methods of dynamic tensile testing and their respective strengths.

Additionally, the author determined that if the dynamic spall experiment is correctly setup, one-dimensional wave theory may be assumed. The effect of stress triaxility was determined to be negligible. The author also determined that the strain sensitivity of the material is due to the material properties alone, not the structural effects (as was proposed).

CHAPTER 3

EXPERIMENTAL SETUP

To verify the capability of achieving the "isosceles triangle" shaped wave (see "A New Theory for Kolsky Bar Dynamic Spall Tests", Chapter 2) using pulse shapers, preliminary tests were performed at the University of North Texas. Subsequent testing as well as analysis of results were performed at the University of Florida Research & Engineering Education Facility (UF-REEF). The setup for the modified Kolsky bar was constructed in a similar manner at both locations.

Modified Kolsky Bar

The optical tables onto which the Kolsky bar was mounted were purchased first and professionally installed, balanced and aligned. The three basic Kolsky bar components: the loading device, the bar components and the data acquisition assembly, were then installed in sequence.

Installation

The barrel was custom made out of hot-rolled 4340 steel. The outer diameter was precision ground to 1.45" and the inner diameter was precision ground to 1.0". The barrel was mounted to the optical table using custom housings made from aluminum 6061 (see Fig 3.1).

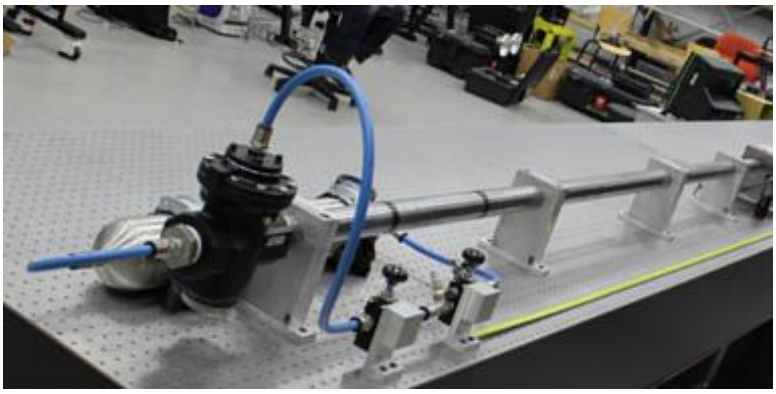

Figure 0.1 Barrel mounting and firing setup

Next the incident bar was purchased. The incident bar and striker were made from C300 Maraging Steel and precision ground to a straightness of 0.002”/ft. and a diameter of 0.0750”. The “impact” end of the bar was implemented with ¾-16UNF-2A threads. The incident bar was mounted to the optical table using linear bearings atop custom aluminum mounting blocks and 0.001” aluminum shims. Custom compression-fitting sabots were purchased with an inner diameter of 0.750” and outer diameters of 1.0”. The sabots were mounted to the striker for precision contact and minimal friction inside the barrel see (Fig 3.2).

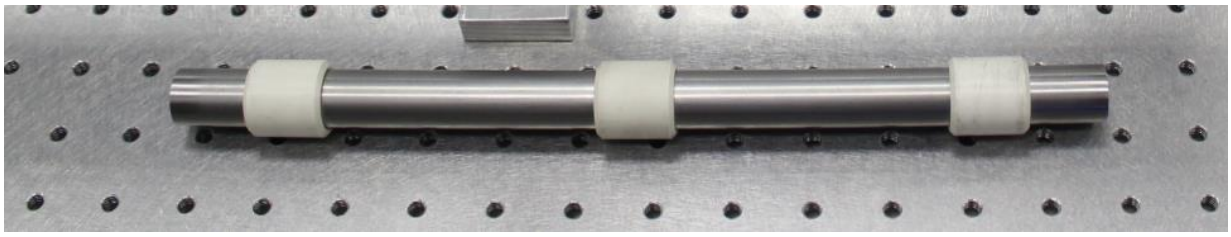

Figure 0.2 Striker with attached sabots

The linear bearings used to support the incident bar were self-aligning so that small misalignments of the bearing housing would not affect the experimental results. Additionally, the bearings were coated with Frelon, and the bar was coated with 3-in-1 oil to minimize friction and wear (see Fig 3.3). Each bearing was mounted to a custom machined aluminum mounting block that was bolted to the optical table. The height of the bearing mounts were each individually

measured and shimmed to 0.001” precision so that the bar’s centroid was constrained exactly five inches above the optical table.

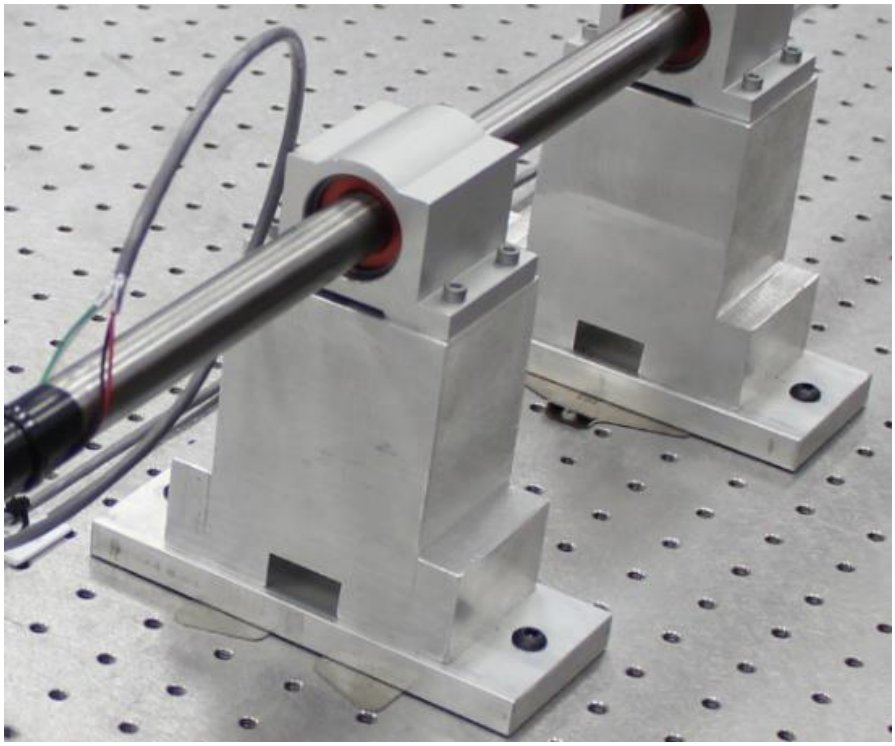

Figure 0.3 Linear bearings, mounting blocks and shims

Once the barrel and incident bar were mounted, they had to be aligned with each other. The striker was placed inside the barrel with a small portion protruding. The protruding striker was used as a reference to align the barrel and the incident bar. Minor adjustments were performed until the contact between the striker and incident bar ends were flush (see Fig 3.4). The alignment was checked by attempting to insert a 0.001” shim between the bars at the interface. The bars were considered aligned when no penetration was possible by the shim (i.e. the striker and bar faces were perfectly flush with each other). This alignment would be further verified using strain gages once they were installed (see “Calibration and Data Reduction”, Chapter 2).

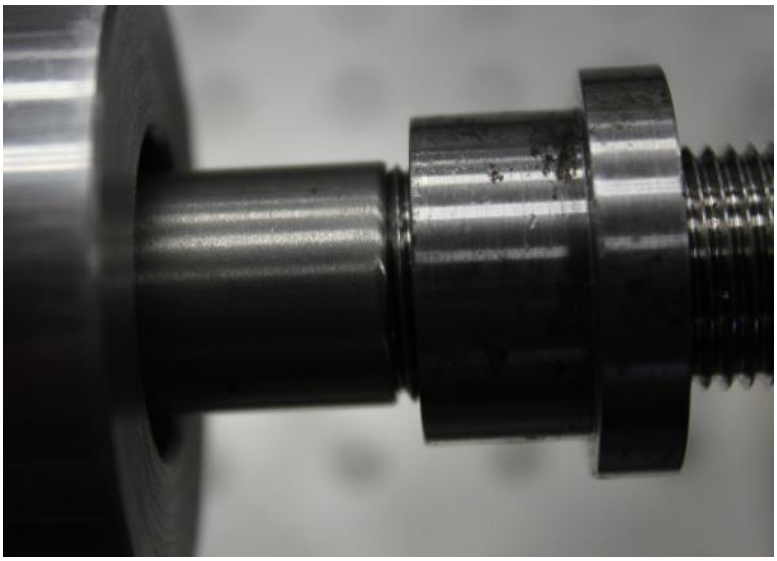

Figure 0.4 Striker aligned with incident bar

After alignment of the barrel and bar, the pressure vessel and valve system were installed. The layout and location were determined to minimize distances and subsequent pressure loss in the hoses. The air tank was mounted behind the barrel, while the button valve and release valve were mounted in front for easier access. The hoses were run behind and below the barrel to help minimize obtrusion (see Fig 3.5). The air compressor line inlet was connected and used for charging the tank and actuating the valve.

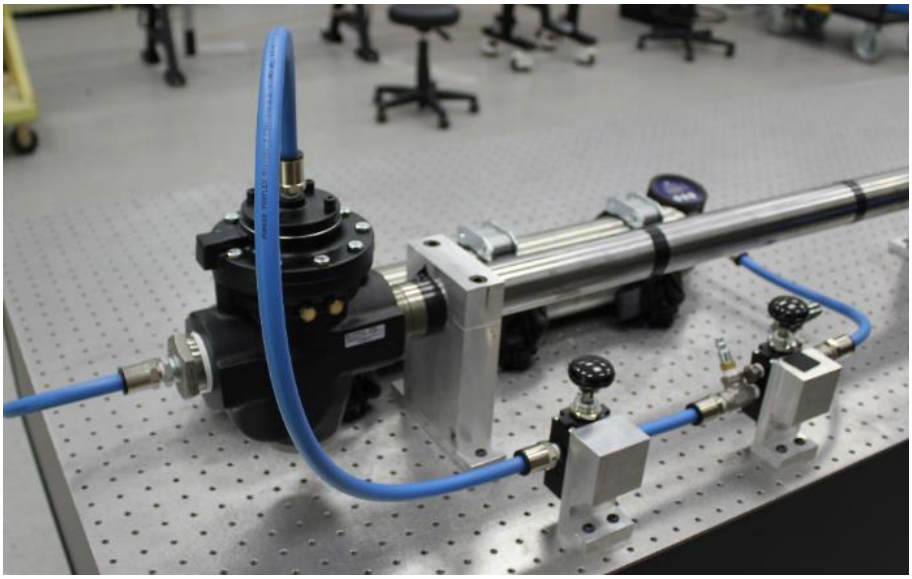

Figure 0.5 Firing assembly

A reproduction of the momentum trap by Song and Chen was drawn by Collin Loeffler and machined by Dynamic Systems Research. The momentum trap was installed in front of the barrel. The incident bar was run through the momentum trap (without touching). A flange (also machined by Dynamic Systems Research) was threaded onto the protruding end of the incident bar (see Fig 3.6). This trap was used to stop the excessive motion of the incident bar due to the wave reverberation.

Figure 0.6 Momentum trap with incident bar (and attached flange) protruding

Strain Gages

The properties of the selected strain gages included a gage factor of 2.08 and a grid resistance of 1000 ohms. The strain gages were seven millimeters long and were mounted 2161-2168 mm from the sample end of the incident bar. The strain gages were mounted using a two-part epoxy to adhere them directly to the incident bar surface. Pairs of strain gages were mounted

180 degrees from each other. Each strain gage was carefully installed to insure parallel orientation with the bar. Once the epoxy cured (overnight), the leads were carefully soldered to wires that were run to the Wheatstone bridge. The leads were given an inverted "U" shape (to alleviate possible axial strain buildup during the motion of the bars), and then secured to the incident bar using electrical tape and zip ties (see Fig 3.7).

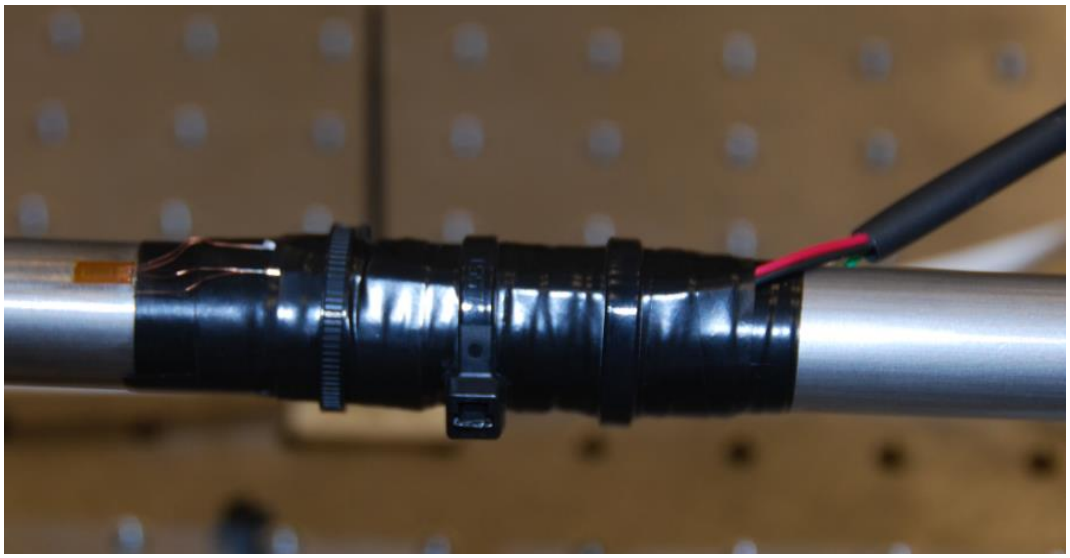

Figure 0.7 Strain gages attached to incident bar

Specimens

Specimens were provided by the Army Engineer Research and Development Center in Vicksburg, MS. Dr. William Heard and Brett Williams cored and precision lapped samples 16" long and 0.75" in diameter, on a lapping machine. The samples were also precision faced and polished on the ends to insure good contact with the bars.

A V-shaped holding device was designed to support the specimen during the impact test. In order to precisely align the specimen with the incident bar, translation stages were attached

(see Fig 3.8). Between the V-shaped holder and the translation stage is a custom-made adapter to allow the proper connection (see Fig 3.8). A CAD drawing showing the design specs may be viewed in Appendix B.

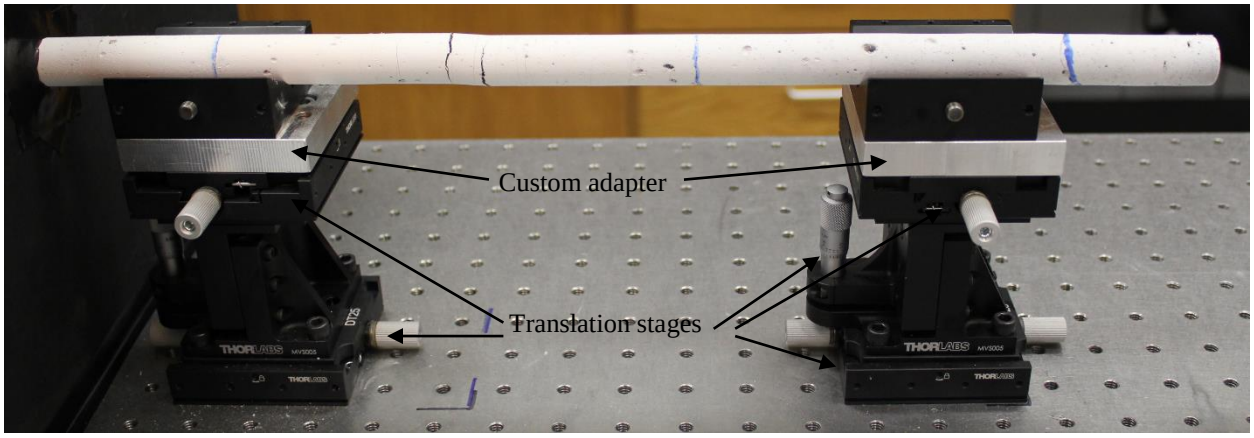

Figure 0.8 Specimen holders with translation stages and custom adapters

Shield

Due to the dynamic nature of the experiments, a protective shield was designed to contain any potential debris during the event. A box was designed from impact resistant Lexan that was sent off for precision machining and then assembled using high grade epoxy.

Momentum Trap

During a spalling event, the specimen breaks apart and the end fragment is “pulled” away by the tensile force. This end piece has the potential to become a projectile. To safely accommodate this, a momentum trap (normally used on a compression bar setup) was placed on the backside of the sample. An initial setup using a glass sample can be seen in Fig 3.10

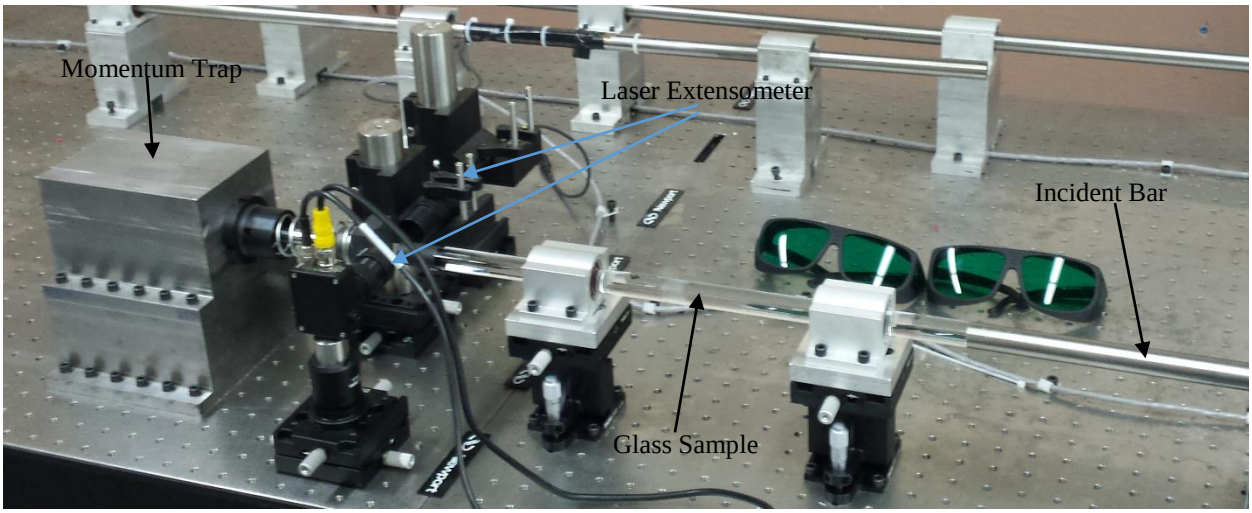

Figure 0.9 Spall setup showing momentum trap

Pulse Shapers

For this project, two materials were used for pulse shaping, annealed copper and Teflon. Pulse shapers were prepared using various diameter hole punches for the copper and Teflon, as well as varying thicknesses.

Sizes and thicknesses of materials used varied for both pulse shapers. Teflon was sampled from sheets that were either 0.01” thick or 0.02” thick. Punch diameter sizes ranged from 1/8” to 3/8” in 1/16” increments. Annealed copper sheets ranged from 0.37 mm thick up to 1.00 mm thick in approximately 0.10 mm increments. Punch diameter sizes ranged from 5/32” to 3/8” in 1/32” increments. All pulse shapers were carefully analyzed to ensure consistency.

When using a hole punch for the copper, the resulting discs were often slightly deformed. In order to ensure consistency with performances, an arbor press was used on every shaper to ensure a consistently flat shape for the pulse shapers. Care was taken not to plastically deform the pulse shapers beyond flattening them into a consistent form.

Laser Extensometer

The laser extensometer setup consists of a fan-beam laser, 2 lenses and a photo detector (or receiver). The lenses used were one inch in diameter and had a two inch focal length. The laser was a fan beam laser and was mounted to a bi-axial translation stage so that careful,

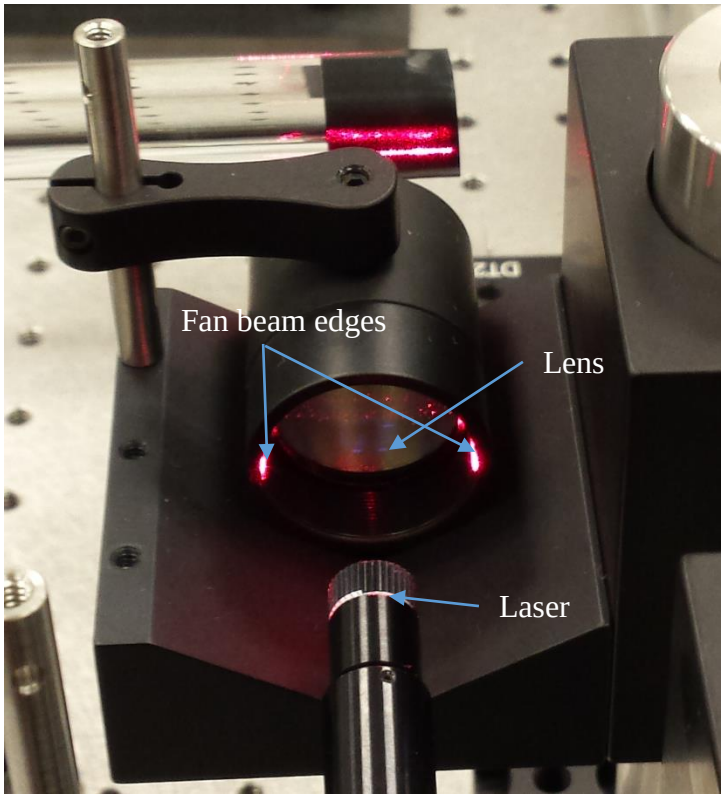

Figure 0.10 Fan beam laser directed into lens

precision adjustments could be made. One of the lenses was mounted approximately two inches in front of the laser. This was the distance determined to capture the laser when the fan reached the lens width of approximately one inch (see Figure 3.11). This lens was also mounted to a bi-axial translation stage in order to be able to make fine, precision adjustment.

The laser beam was refracted from the lens to have a parallel orientation upon leaving the lens housing. This flat “board shaped” beam is what was used to track the displacement of the spall specimen. The focal length of the beam leaving the lens was two inches. The beam shaped

laser was maintained, but the thickness changed due to the lens refraction. Another lens mounted in front of the receiver (again, by two inches) corrected the beam and refocused it into the receiver (see Fig 3.12). The second lens and receiver were attached to each other with an aluminum tube at the lens focal length distance. The receiving unit (lens plus detector) was

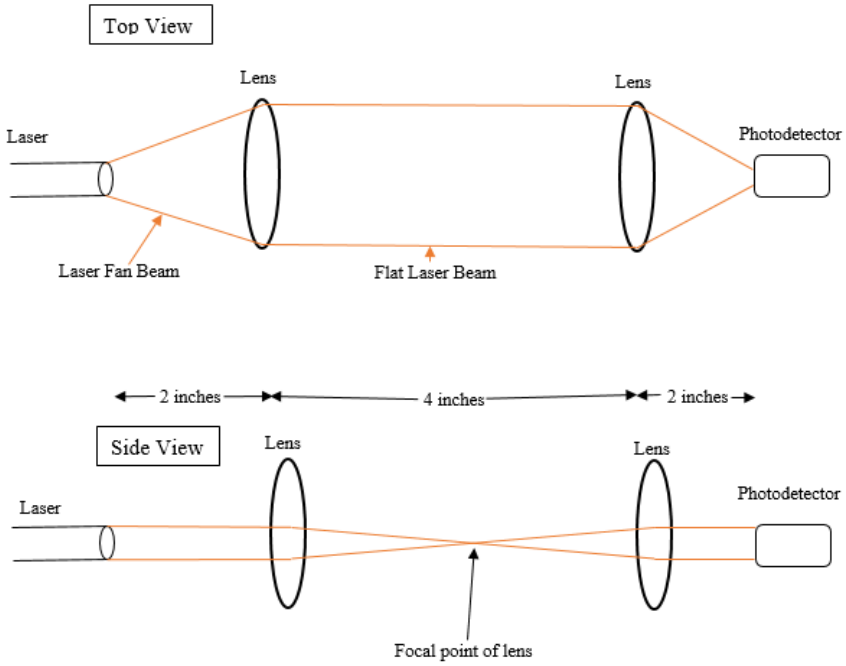

Figure 0.11 Schematic showing top and side views of laser optics

mounted to a bi-axial translation stage to allow precision modifications. The complete setup spanned approximately 12 inches. The four inch gap between the two lenses is where the specimen is positioned. The translation stages were carefully moved until the laser setup was perfectly aligned and all beams and lenses were at their proper distances. The translation stages were locked in place to prevent any adjustments during experimentation.

Once the laser setup was in place, the laser needed to be calibrated. A device was needed to model the displacement of a specimen as it passed between the lasers. The model was created with a hollow tube mounted to a horizontal translation stage (see Fig 3.13). The tube was

positioned to block the laser from receiving any light from the laser. The receiver was connected to an oscilloscope so that the output voltage could be recorded. The tube was then moved 0.005" in step size on the translation stage with the corresponding voltage output being recorded. This process was repeated until the tube no longer blocked any of the laser. The model measurements were converted from inches to millimeters and then the slope and R^2 value of the displacement-voltage correlation were graphed. The data was truncated from both ends of the slope until a R^2 value of at least 0.9998 was reached. This represented the range in which the laser could be used to calculate the displacement. An example showing the relationship (slope, or L_s) and consistency (R^2 value) is shown in Fig 3.15. The setup was considered calibrated once the range and laser sensitivity were determined.

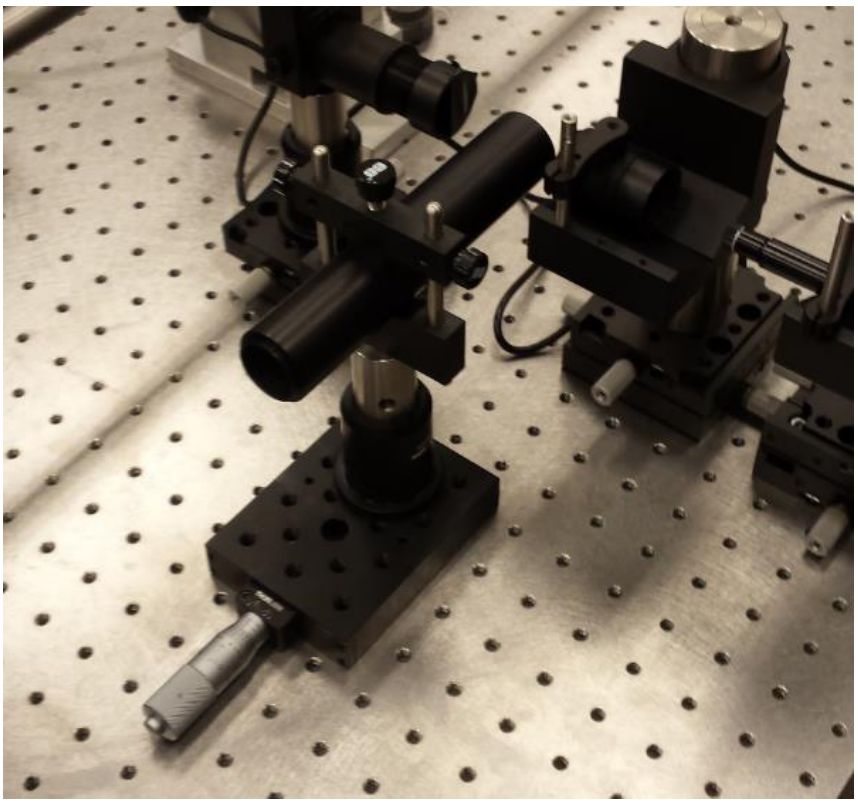

Figure 0.12 Specimen calibration model on translation stage

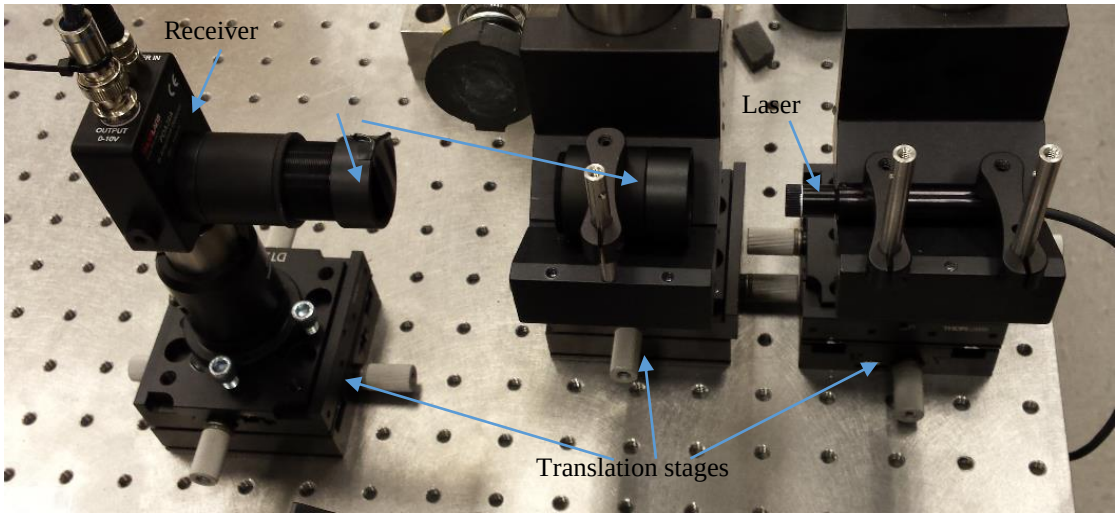

Figure 0.13 Laser setup

It was determined during experimentation that the light from the flash of the high speed camera was affecting the laser receiver readings. Because of this, a makeshift box had to be constructed and sealed over the laser setup to keep the light from affecting the photodetector readings (see Fig 3.16). The laser was then recalibrated due to the differences in light setting.

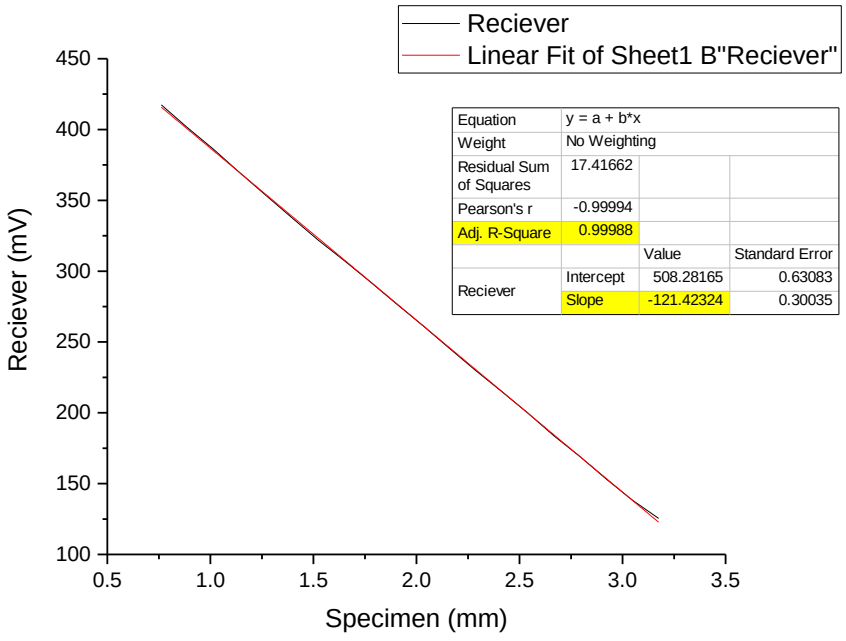

Figure 0.14 Graph showing laser sensitivity (slope)

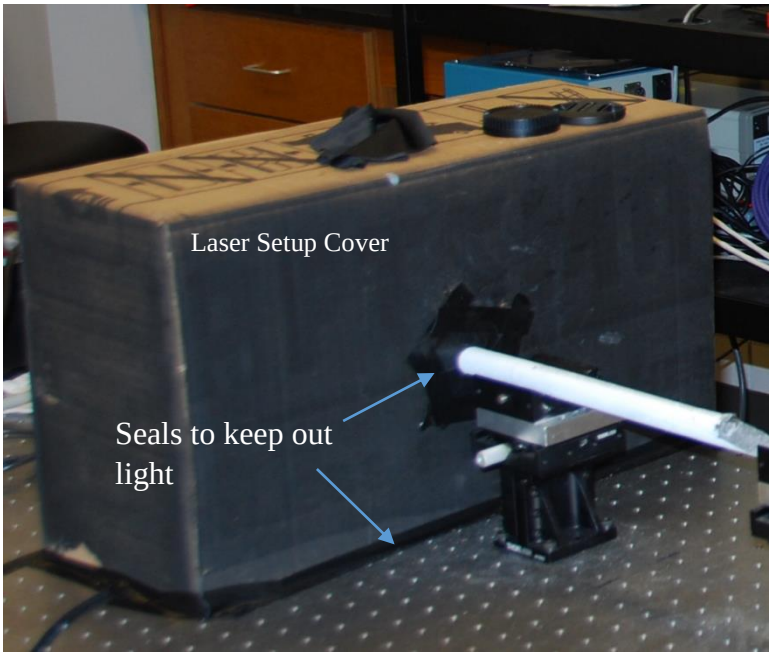

Figure 0.15 Makeshift box covering laser setup

DIC

High-Speed Videography

For all videography in this project, a Kirana camera was used with a Nikon lens. The setup consisted of a camera, a (sturdy) mount, lighting/flash equipment required for the camera, and the cables connecting them to a laptop and an oscilloscope. Since the event took place in the span of a few milliseconds, determining the flash and trigger timing took a couple of days of trial and error to adjust correctly.

1) Flash

Since the exposure time for each frame was only a few microseconds, the event had to be extremely well lit in order for the camera to process the images. The Kirana cameras came with LED lights to use for filming (see Fig 3.17). Because of the high frame rate (200,000 frames per second) that was used, the LED lights did not provide sufficient intensity. After many attempts it became clear that the lighting provided by the LED bulbs was too dim.

The second option for lighting was to use flash bulbs. It took many trials to get the flash intensity and duration correctly set up so that the event was clearly visible. Since the flash bulbs are not continuous, the flash also had to be triggered during the event.

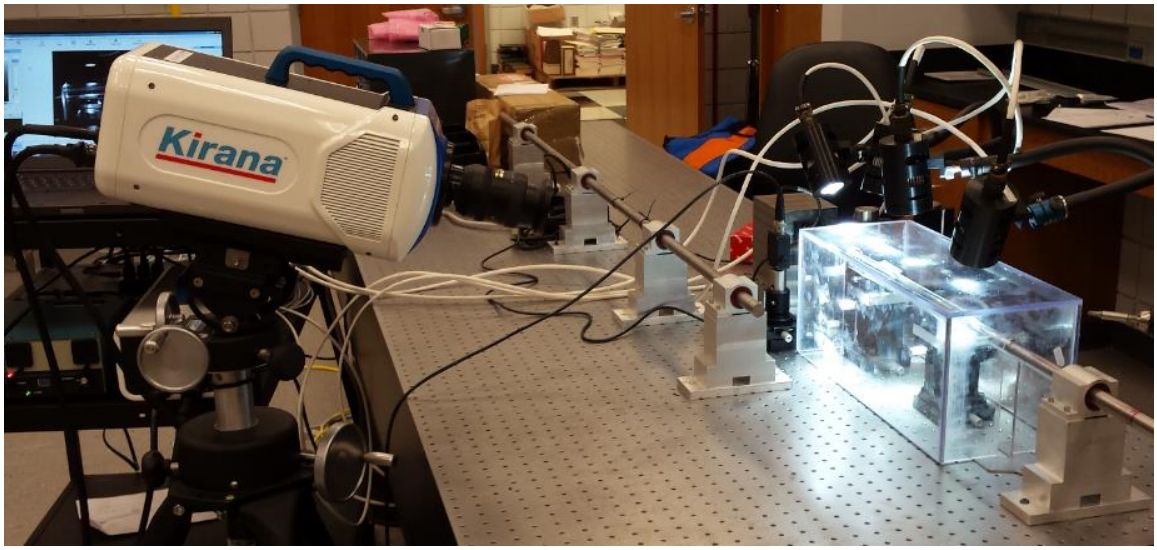

Figure 0.16 Camera and LED light setup

2) Timing

Once the flash bulbs were determined to be necessary, an appropriate triggering and timing mechanism had to be implemented. Three different triggering mechanisms were explored to determine the best fit.

The first choice was to use custom lasers that were previously purchased for the purpose of measuring striker velocity. The lasers were set to trigger when the striker interrupted the laser path as it exited the barrel (see Fig 3.18). The laser receiver was connected to the oscilloscope, as were the flash bulbs. The bulbs were then set to flash when the laser signal reached a threshold value (i.e. the laser path interrupted by the striker) on the oscilloscope. The laser setup functioned, but required constant monitoring of the lasers, and the timing of the flash was difficult to get consistent. A better approach was necessary.

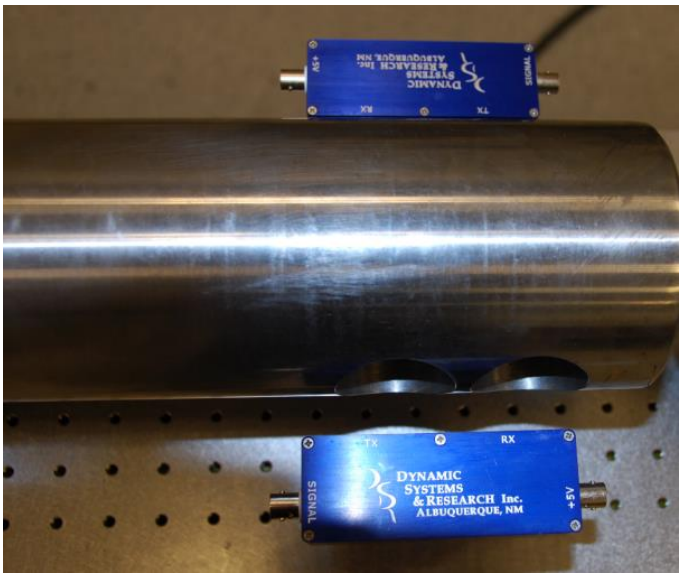

Figure 0.17 Laser signal setup

Our second choice was to use the strain gauges as the trigger. Since the strain gages were already connected to the oscilloscope, only the flash had to be adjusted to the correct timing of the incident pulse. This setup was a good idea and would have worked well except for the timing. The trigger of flash needed to be slightly delayed to better synchronize with the spall event. This was not possible to configure by directly using the strain gage signals, so another option had to be explored.

The third option consisted of using the strain gages as a trigger, but sending the signal to a sequencer for triggering (a splitter was used since a signal also needed to be sent to the oscilloscope). After many practice runs, this setup proved to be the most effective.

Once the flash and trigger were determined, the following conditions were determined for the experiment:

- Frame rate: 200K FPS
- Exposure: 1µs
- Camera delay: 300µs

- Flash intensity: 177 ($1/8^{th}$ power)

DIC

For digital image comparison, an expert from Correlated Solutions (the manufacturer of the software) flew out to the UF-REEF to give a two day presentation on how to use the software and operate the cameras. The cameras had to be carefully set up and calibrated, the specimens had to be carefully prepared, and the software had to be learned.

1) Camera setup and calibration.

The cameras were mounted to a custom stand that was designed to have the cameras offset to each other, both focusing on the same area (see Fig 3.19), therefore getting a specific camera angle was not necessary.

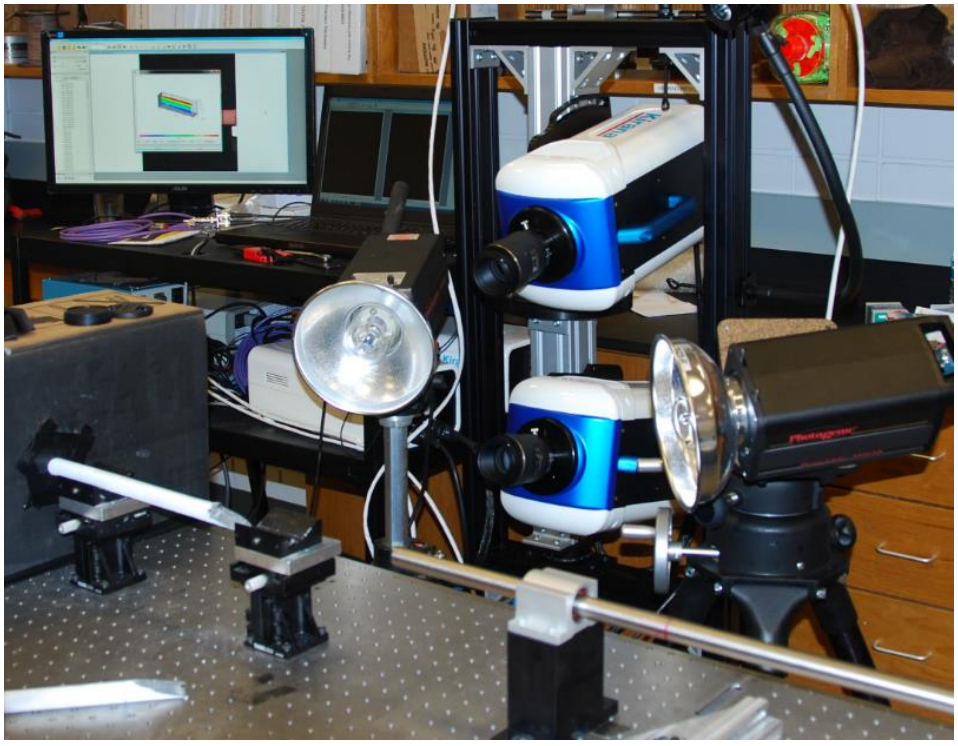

Figure 0.18 DIC setup showing cameras, flashes and software

Calibration was done using the software and the calibration substrates that came with the DIC purchase from Correlated Solutions. A calibration plate was placed where the event would occur, and the cameras focused to it (see Fig 3.20). The plate was then rotated about all three axes (6 degrees of freedom) as the cameras took simultaneous pictures. The pictures were then used by the software to synchronize the cameras to each other.

Figure 0.19 Correlated Solutions calibration substrate

2) Specimen preparation

The DIC software functions by recognizing contrasting images on the specimen and then tracking their relationship to each other. In order to do this, the specimens were painted white and then given a black speckled pattern. Initially this was accomplished by spattering paint onto the sample. Getting the spatter droplets to the ideal size range was difficult and took practice. Overspray also caused difficulty by shading the specimen. Several experiments were performed in this manner before the expert from Correlated Solutions proposed an alternative solution.

Since the spray paint method was providing inconsistent results, it was suggested that each individual speckle be hand drawn with a permanent marker (see Fig 3.21). This created

more consistent results by giving greater contrast. Each specimen was then hand speckled in preparation of the experiment.

3) Software

During a dynamic test the software tracks the displacement of each speckle individually, as well as with respect to that of its surrounding speckles. By doing this, the software calculates strain ($\frac{\Delta l}{l}$) of the object in each direction. Furthermore, the camera tracks speckle movement frame by frame, which are captured at a preset speed. Using this information, the software can take a time derivative of the strain to calculate the strain rate. A DIC picture of a specimen with a superimposed strain distribution is shown in Figure 3.21.

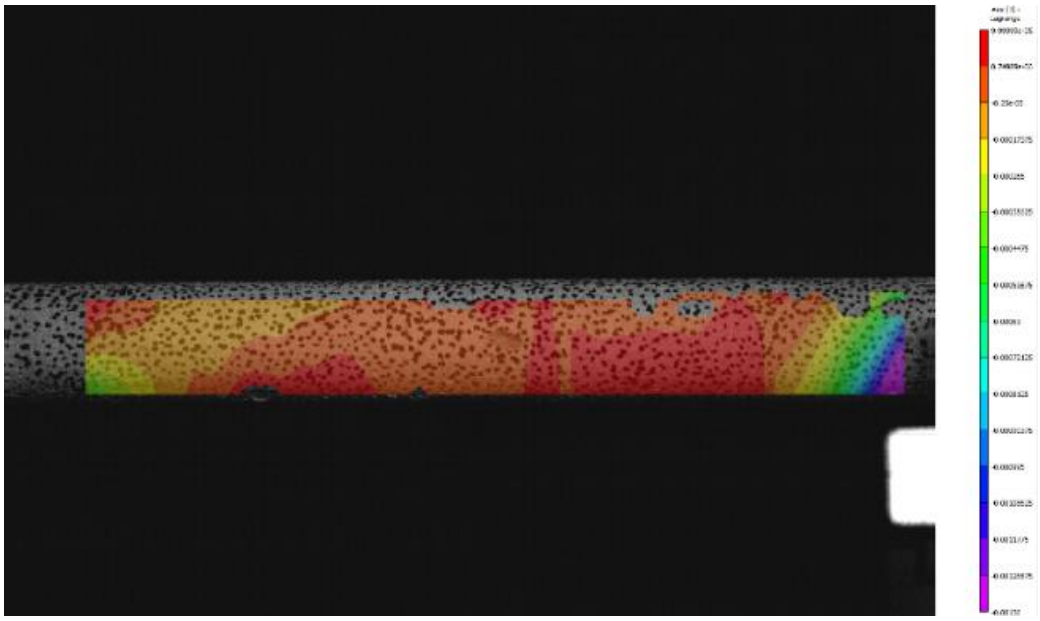

Figure 0.20 Speckled specimen with superimposed strain calculation

CHAPTER 4

RESULTS, ANALYSIS AND DISCUSSION

Preliminary data was needed before commencement and analysis of the experiment. Establishing and verifying boundary conditions were performed first, and then the experiments.

Initial Conditions

The initial parameters that needed to be established were: wave speed in the bar, wave speed in the specimen, and striker velocity.

Wave speed in bar:

The wave speed in the bar was determined by placing strain gages at two different locations on the incident bar that are two feet apart. Initiating the striker impact allowed the resulting stress waves passing through both strain gage locations with the respective waveform (and timing) being recorded by the oscilloscope. Taking the distance between the strain gages and dividing it by the time gave the wave speed of the bar. In this experiment, the wave speed was determined to be 4950 m/s. This is close to the published value of 5000 m/s for the bar material.

Wave speed in the specimen:

The wave speed in the specimen was provided by the Army Engineer Research and Development Center (ERDC). For the specimens provided, the wave speed was given as 4550 m/s.

Striker velocity:

The striker velocity had to be measured after the desired wave form was achieved. For the striker velocity, a laser system was set up (see Fig 3.18). The laser box has two lasers connected

to the oscilloscope. Similar to the wave speed, the striker speed was calculated by dividing the distance between the lasers by the time it took for the striker to reach each one as recorded by the oscilloscope. For the lab at the UF-REEF, under the ideal pulse shaping conditions, the striker velocity was determined to be 14.03 m/s.

Achieving the Correct Wave Form

The most significant goal of this project was to verify theoretically (see *A New Theory for Kolsky Bar Dynamic Spall Tests,* Chapter 2) and experimentally that the required wave form could be achieved. This was initially achieved at the University of North Texas (UNT). After firing over a hundred shots using an array of pulse shaper sizes and configurations, an acceptable wave form was determined using the following parameters: the striker was placed 3.5' into the striker, the pressure vessel was charged to 40 psi, an 11/32" annealed copper pulse shaper 1.0 mm thick was "stuck" to the incident bar using petroleum jelly, and a 1/8" Teflon pulse shaper 0.02" thick was placed on top of the copper pulse shaper also using (minimum) petroleum jelly. Using these parameters yielded the waveform seen in Fig 4.1. The following shows that this wave form falls within an acceptable range (>4% difference) of symmetry.

$$\frac{3.947 - 3.852}{\left(\frac{3.947 + 3.852}{2}\right)} * 100 = 2.44\%$$

Further experimentation was not carried out until arrival at the UF-REEF.

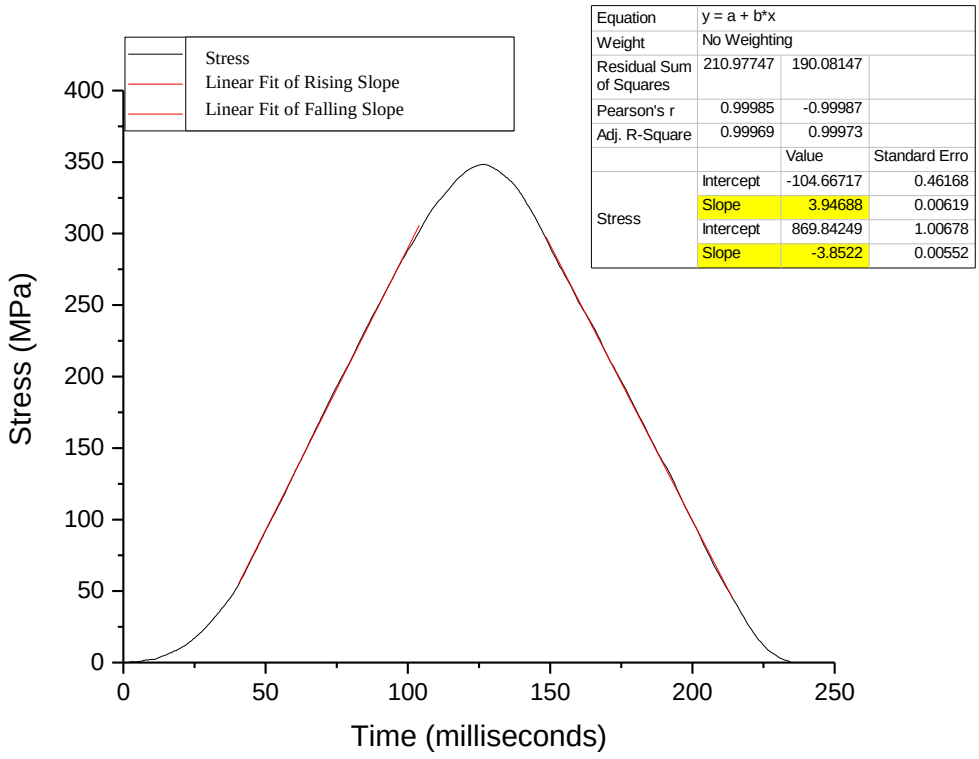

Equation	y = a + b*x		
Weight	No Weighting		
Residual Sum of Squares	210.97747	190.08147	
Pearson's r	0.99985	-0.99987	
Adj. R-Square	0.99969	0.99973	
		Value	Standard Erro
Stress	Intercept	-104.66717	0.46168
	Slope	3.94688	0.00619
	Intercept	869.84249	1.00678
	Slope	-3.8522	0.00552

Figure 0.1 Wave form showing slope comparison from UNT

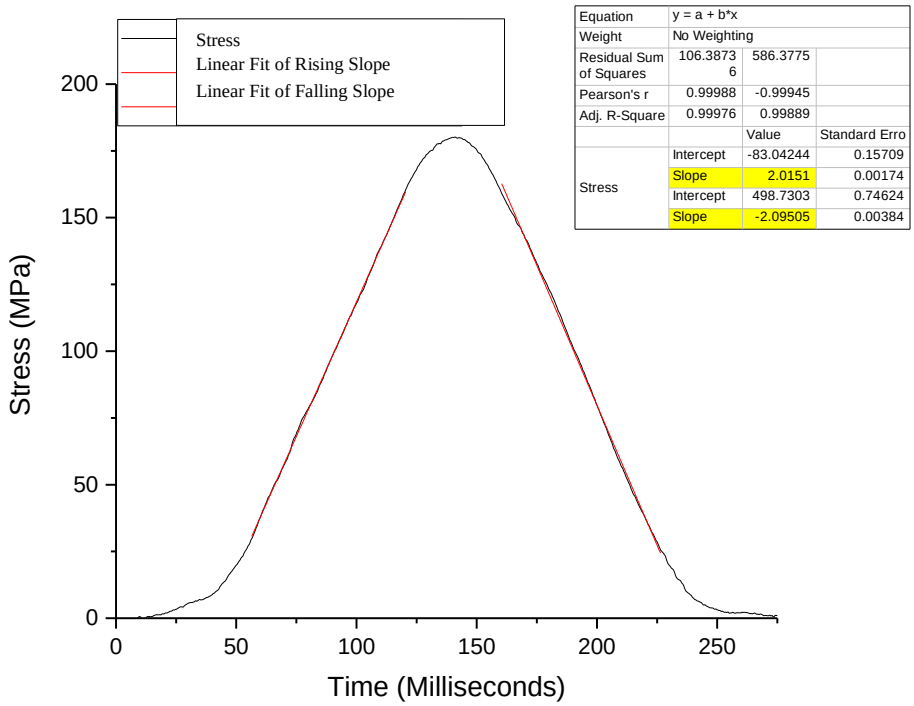

Equation	y = a + b*x		
Weight	No Weighting		
Residual Sum of Squares	106.38736	586.3775	
Pearson's r	0.99988	-0.99945	
Adj. R-Square	0.99976	0.99889	
		Value	Standard Erro
Stress	Intercept	-83.04244	0.15709
	Slope	2.0151	0.00174
	Intercept	498.7303	0.74624
	Slope	-2.09505	0.00384

Figure 0.2 Wave form with slope comparison from UF-REEF

At the UF-REEF, it was assumed that the pulse shaping parameters used at UNT would yield similar results. The barrel at the UF-REEF, however, was two feet longer than the one used at UNT and so different wave forms were realized. The pulse shaping had to be re-established. After experimenting for a couple days, an acceptable wave form was again found. The new parameters were: the striker was placed 5.5' into the barrel, the pressure vessel was charged to 25 psi, a 9/32" annealed copper pulse shaper 1.0 mm thick was "stuck" to the incident bar using petroleum jelly, and a 1/8" Teflon pulse shaper 0.02" thick was placed on top of the copper pulse shaper also using (minimum) petroleum jelly. Using these parameters yielded the form seen in Fig 4.2. Analysis of the symmetry (as performed above) yields 3.89% variance. A series of experiments were compared to verify repeatability (see Fig 4.3).

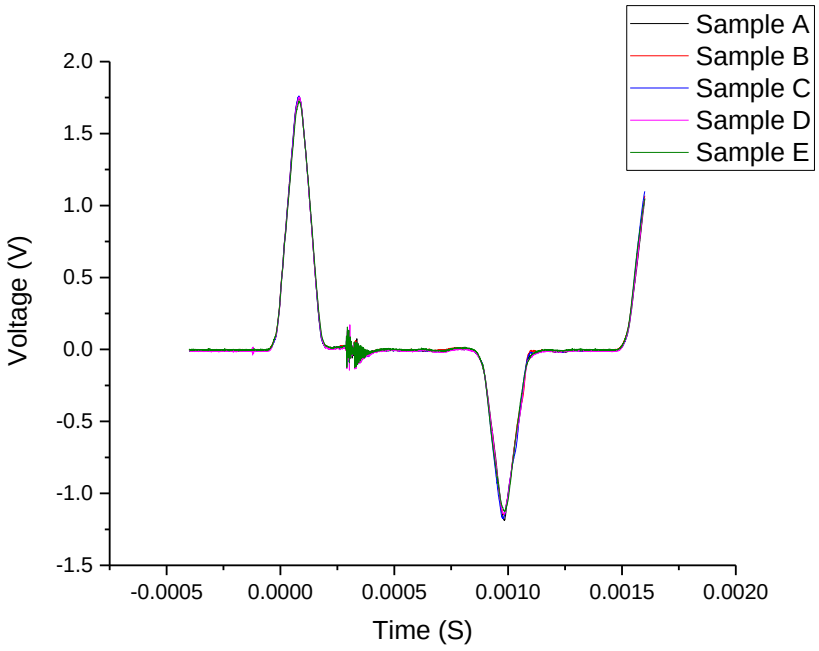

Figure 0.3 Comparison of wave forms to illustrate repeatability

Using these parameters, the striker velocity was determined to be 14.287 m/s using the setup mentioned above.

Determining the Spall Strength

Due to limited concrete samples (and the associated time and expense required to make them), initial testing was performed on sodium borosilicate glass (aka Pyrex). Glass samples were precision made to the same specifications as the concrete samples.

Glass Samples

Initially, experiments were performed using glass samples to verify that the camera, laser extensometer, and strain gages were all working properly. The specimens were placed on V-shaped holders that were attached to translation stages to allow precision adjustments. Each specimen was lined up to the incident bar in the same way that the incident bar was aligned to the striker (see Fig 4.4). Once the specimen was satisfactorily aligned, a small amount of vacuum grease was applied between the incident bar and specimen faces in order to eliminate possible small gaps at the interface. The wave form for the glass sample can be seen in Fig 4.5. Additionally, a frame from the high-speed camera showing the glass fracture may be seen in Fig 4.6. The camera allowed made it possible to watch the event and see where the initial (tensile) crack formed – information necessary for later analysis. After the event, pieces that fractured during the initial tensile wave were identified by unique striations in the fracture pattern. After the initial failure, stress waves propagated throughout the specimen causing multiple additional failures under "random" wave direction and stress/strain conditions. Analysis of the fractured pieces showed vertical striations on the initial crack section, verifying that the sample failed in tension. For a comparison of tensile failure and failure due to random other stress waves, see Fig 4.7.

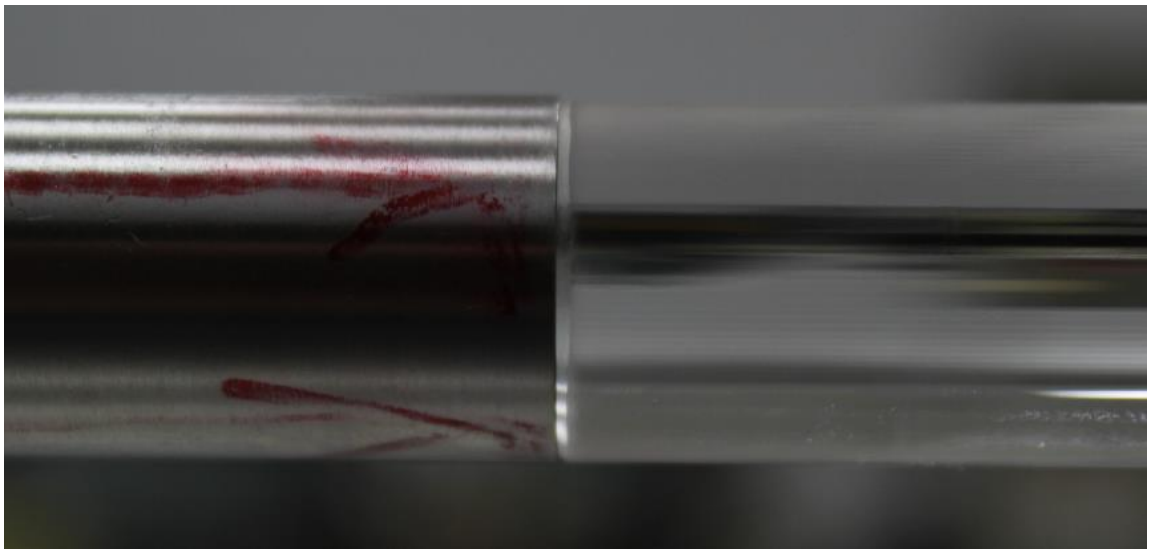

Figure 0.4 Alignment between incident bar and glass sample

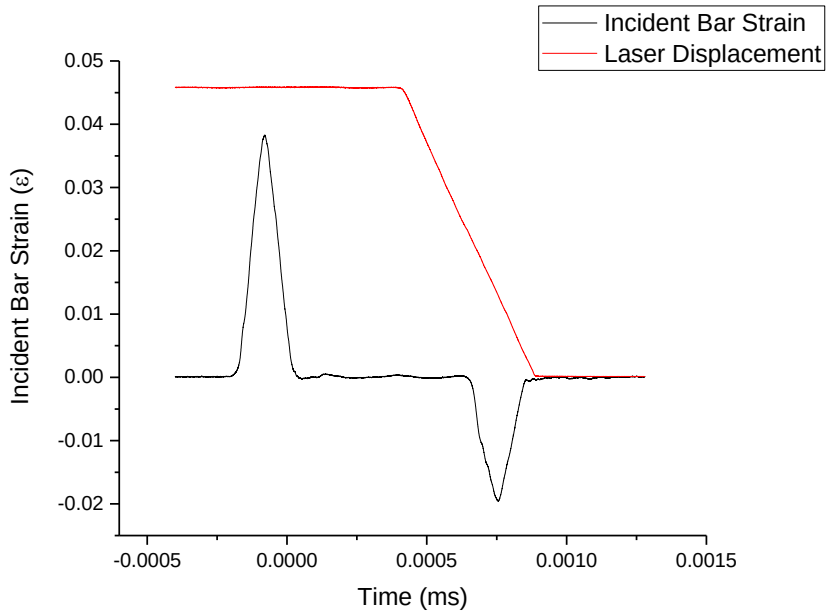

Figure 0.5 Strain plus displacement in glass specimen

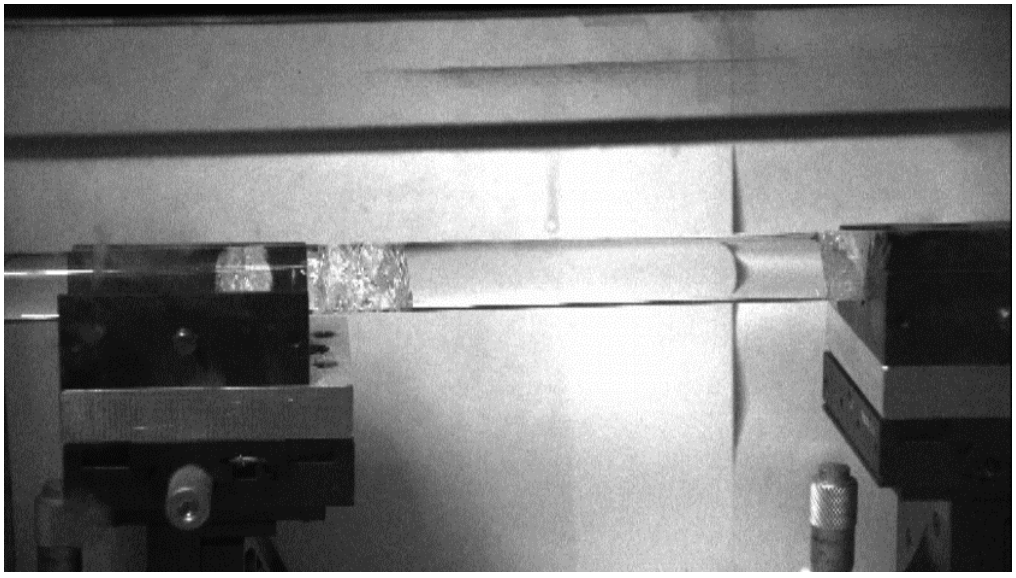

Figure 0.6 Glass sample showing failure during event

Figure 0.7 Figure showing (a) tensile failure striations and (b) random failure

Concrete Specimens without DIC

Experiments on the concrete specimens began using the laser extensometer and high-speed camera only (no DIC). Some of the samples failed in compression due to manufacturing defects. Failures in compression were caused by shear cracks shown in Fig 4.8 and were easily identified.

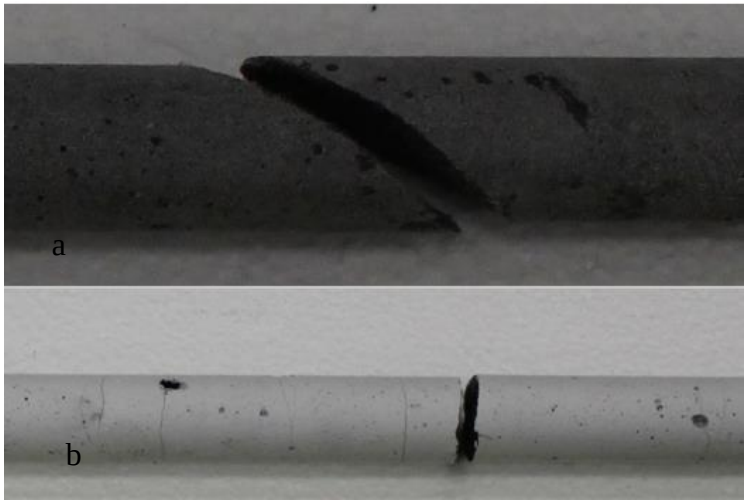

Figure 0.8 Figure showing (a) specimen failure in compression and (b) specimen failure in tension

A total of 12 samples were tested using this setup, out of which 7 fractured under tension. After verifying that the experiments had the correct waveform, these samples were analyzed using the laser extensometer and the high-speed camera data.

The first step in analysis was to analyze the camera footage and determine where the initial crack formed (see Fig 4.9). This information was necessary for calculations. Each (good) specimen was carefully analyzed and a simple excel spreadsheet was used to record the distances from the initial crack to the free end of each sample, called the “spall distance” (see Table 4.1).

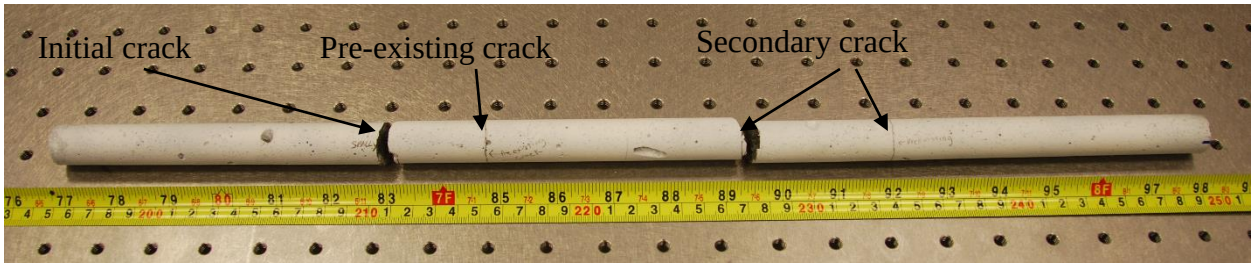

Figure 0.9 Valid sample with cracks identified

Table 0.1 List of spall distances of specimens

File	Distance to Fracture (mm)
6_25_glass1	140
6_30_Concrete1	150
6_30_Concrete3	85
7_1_Concrete1	205
7_1_Concrete2	158
7_1_Concrete4	143
7_6_Concrete1	110
7_6_Concrete2	244

After determining the spall distance, the next step in the analysis process was to determine the spall strength using the laser displacement data. Initially, the laser voltage was divided by the laser sensitivity factor to get distance, and then plotted against time (see Fig 4.10).

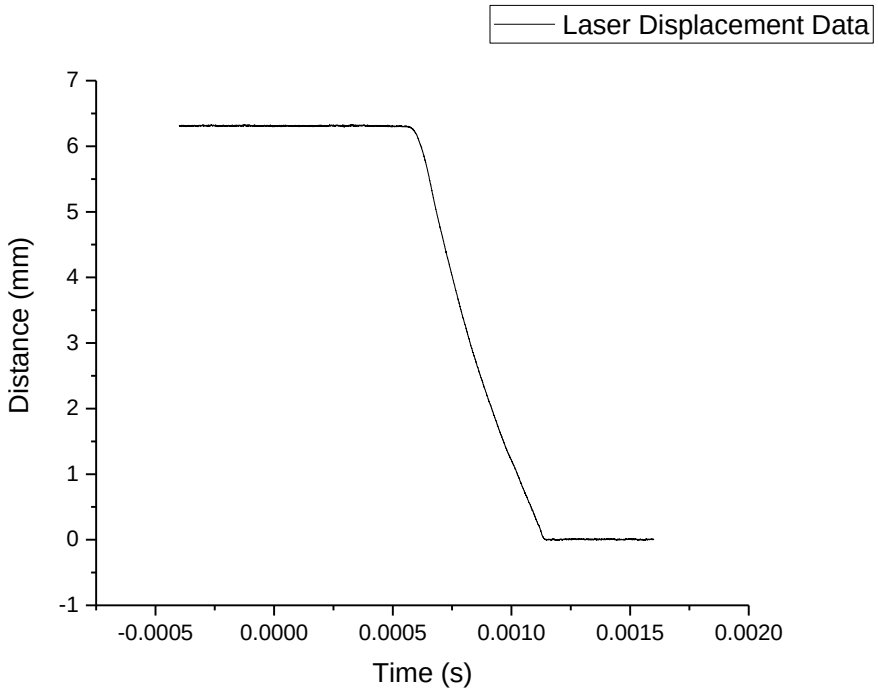

Figure 0.10 Specimen displacement from laser data

Once the displacement and time were known, a single time derivative was taken to give velocity (Fig 4.11)

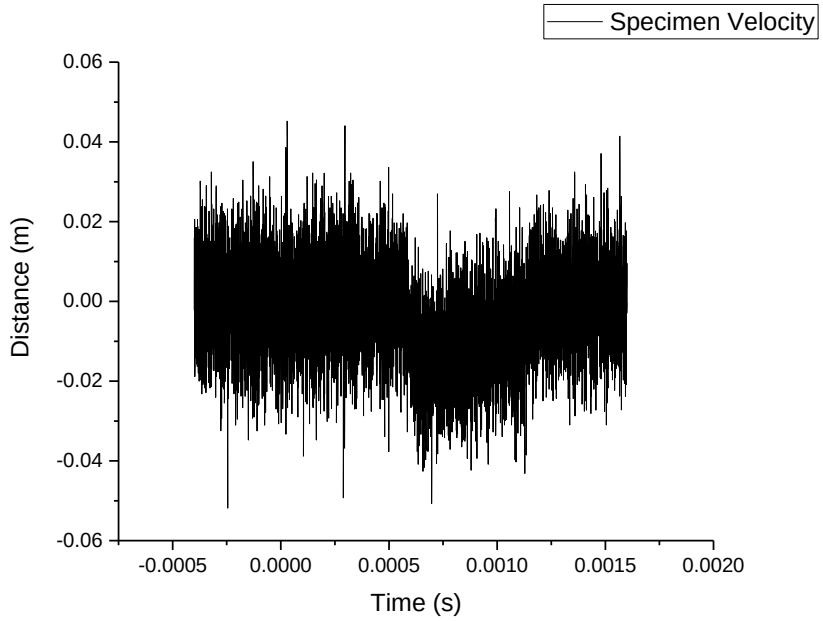

Figure 0.11 Velocity of specimen derived from displacement

The time derivative introduced an unknown amount of error. Because of this, a Fourier Filter was used to find the “relevant” velocity data (see Fig 4.12)

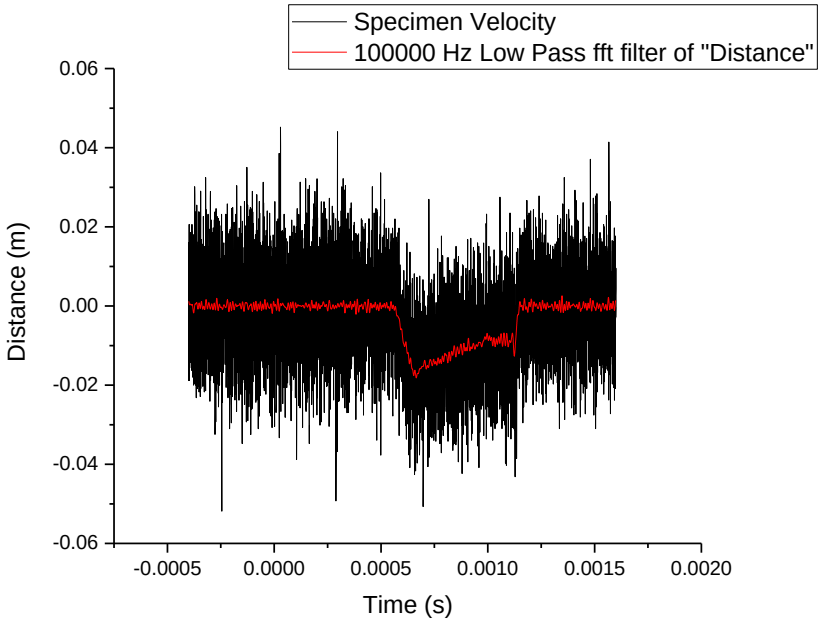

Figure 0.12 Specimen velocity shown with filter applied

Discarding the unfiltered section leaves the velocity/time data for the specimen (Fig 4.13).

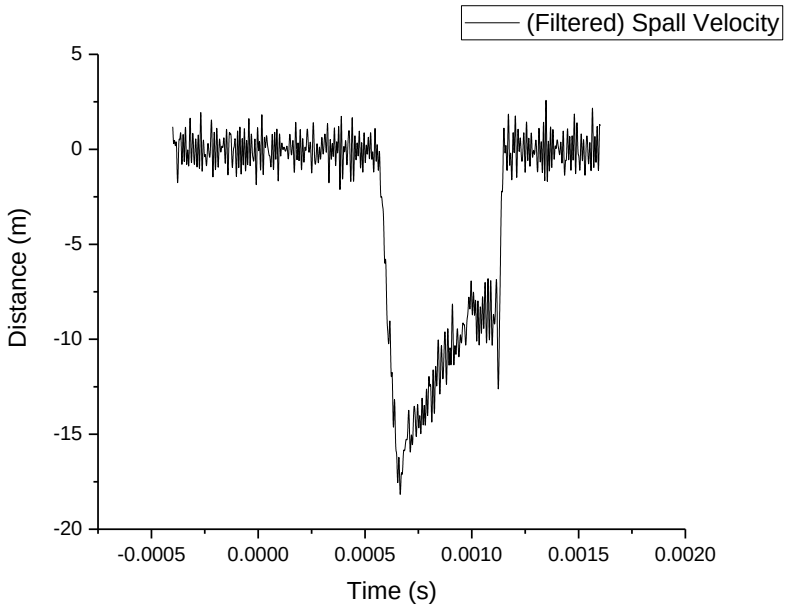

Figure 0.13 Filtered velocity/time data of specimen

Looking closely at the velocity data, it can be seen that there is a deviation point on the "back side" of the initial slope (Fig 4.14). This deviation represents the point at which the specimen initially failed and began to separate (or spall). The velocity at the deviation point, or spall velocity, was then recorded.

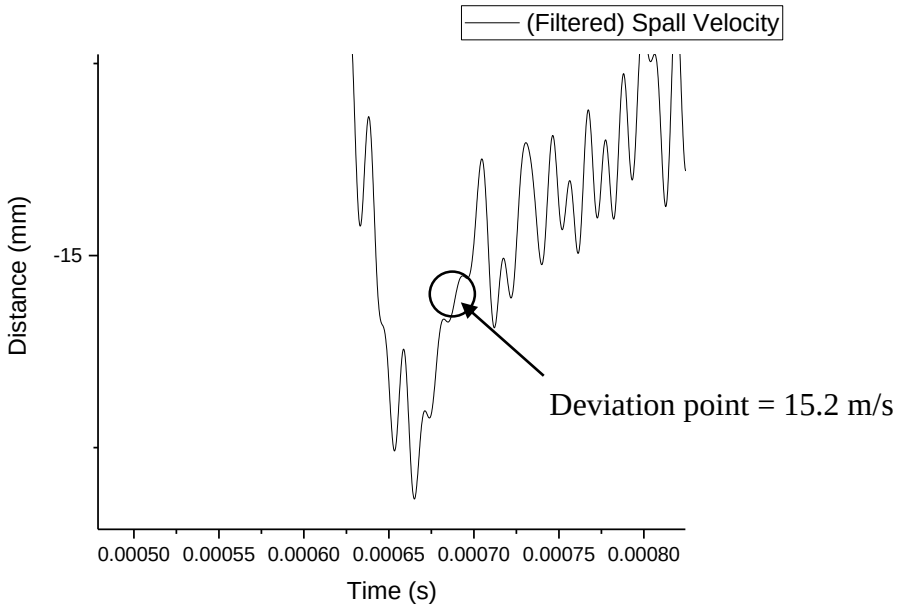

Figure 0.14 Velocity deviation point indicating spall

The next step in analysis was to find the time it took for the wave to travel to the initial crack, and then subtract that from the deviation point to determine the velocity change brought about by the initial crack. This information is directly related to the spall strength.

First the distance to the initial crack is divided by the wave speed of the specimen material (and convert s to μs):

$$\frac{l}{C} = \frac{85\ mm}{4550\ m/s} * \frac{1000\ s}{\mu s} = 18.7\ \mu s$$

In wave mechanics, the velocity at the free end of an object during one-dimensional wave propagation will be doubled [8]. Accounting for this, it is necessary to double the time to get the specimen position during the spall event:

$$18.7 * 2 = 37.3\ \mu s$$

From the recorded data, trace back 37.3 μs on the loading wave from the deviation point. The correlating velocity is 17.2 m/s. Now subtracting these two velocities gives the change in velocity brought about by the spall:

$$\Delta v = 17.2 - 15.2 = \ 2 \text{ M/s}$$

Recall that the specimen velocity doubles at the free end. Now, this must be converted back to the true particle velocity induced by the loading wave:

$$v = \frac{2}{2} = 1 m/s$$

Using equation 2.2 to solve for the spall strength gives:

$$\sigma = \frac{(2200)(4550)(1)}{100{,}000} = 10.01\ MPa$$

Each of the samples were analyzed in like manner to determine the spall strength. The results may be seen in Table 4.2

Table 0.2 Calculated spall strengths of specimens

Specimen File Name	Spall Strength
6_30_Concrete1	12.24 Mpa
6_30_Concrete3	10.01 MPa
7_1_Concrete1	14 MPa
7_1_Concrete2	12.51 Mpa
7_1_Concrete4	12 Mpa
7_6_Concrete1	10.87 Mpa
7_6_Concrete2	15.47 Mpa

After examining the data and analysis for the spall strengths of the specimens, it was noticed that the time derivative introduced a large amount of noise. Since the velocity profile at that point could not be analyzed, a filter was applied, further increasing the error uncertainty for the calculation. Since there is not a good way to know how much data was filtered out, the laser extensometer in general was determined to be insufficient for analyzing spall data.

Concrete Samples with DIC

Once the DIC training was complete, samples were set up to be analyzed using this new technique. 11 specimens were used for the DIC analysis, out of which 5 fractured properly and were used for analysis.

Using the DIC technique, all calculations were performed using the software. The calculations were performed by identifying each individual speckle and monitoring its relative motion to itself and its surrounding speckles during a spall test. Assuming one-dimensional wave propagation, the software was configured to analyze the linear (x-direction) strain. An example can be seen in Fig 4.15.

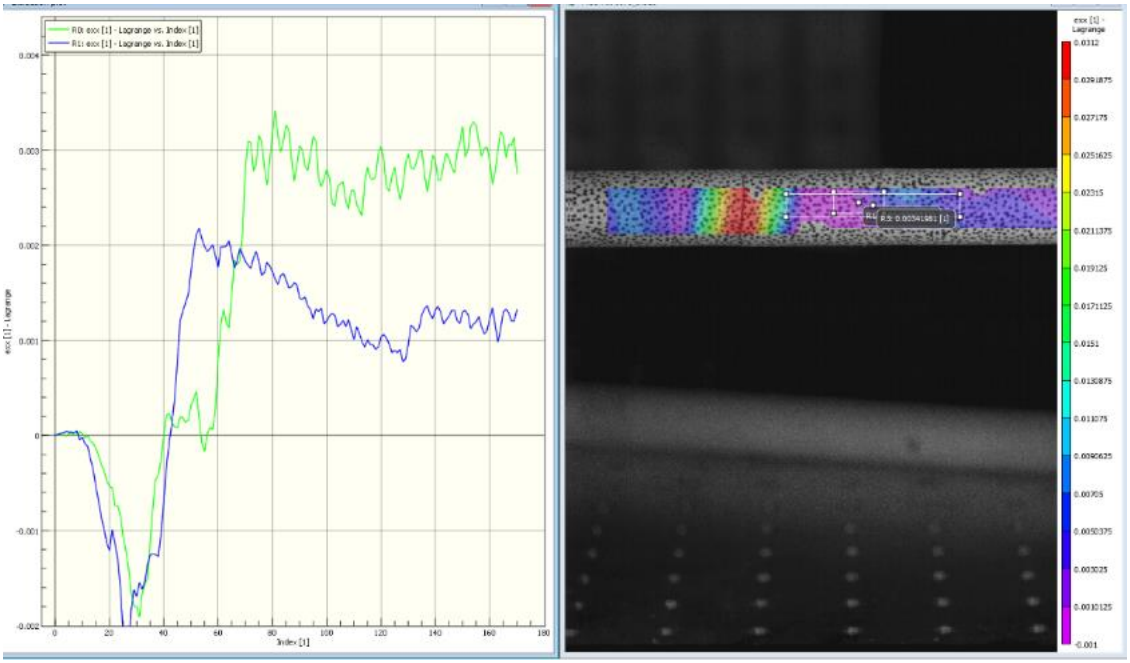

Figure 0.15 DIC software analysis of specimen

Upon close inspection of the DIC results it was determined that the software calculations were inconsistent. It was determined that this was due to the fact that the specimens typically failed at a tensile strain of 0.0002. This deformation was determined to be too small to be consistently detected by the software and so the DIC analysis, like the laser extensometer, was determined to be unsuitable for spall strain analysis.

Determining Strain Rate

Determining the strain rate was achieved by examining the strain gage data. Preliminary data is given in Table 4.3.

Table 4.3 Preliminary conditions for strain rate analysis

Condition	Value
Excitation voltage (V)	15
Gain	100
Bar modulus (GPa)	200
Specimen Modulus (GPa)	45.5
Wave speed in bar (m/s)	4950
Wave speed in specimen (m/s)	4550
Strain-gage gage factor	2.08

The data recorded by the oscilloscope (voltage output from strain gages vs time) was graphed. As an example, the same specimen will be analyzed. In the graph, the incident wave is shown on the left, then there is an inverse wave shown on the right. The inverse wave shown is the reflected wave generated at the incident bar-specimen interface. The difference between these two waves represents the stress transmitted into the specimen (see Fig 4.16).

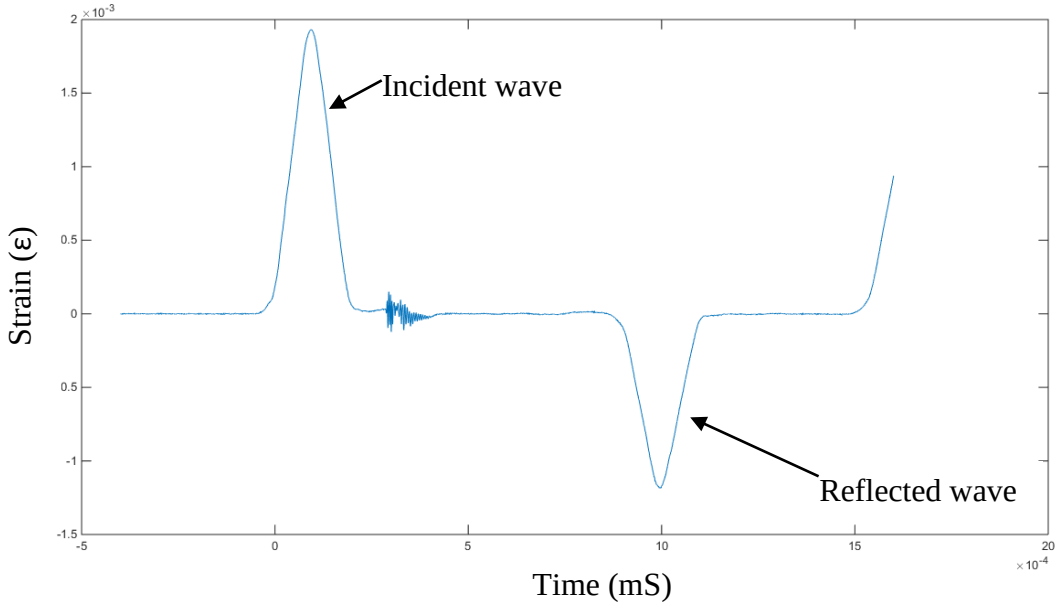

Figure 0.16 Graph of raw data showing incident and reflected waves

A ratio between the two waves was created. Then the incident wave was multiplied by the ratio and Eq 2.1 (with the given parameters above) shown below:

$$Ampl * \left(1 - \frac{ampl\ min}{ampl\ max}\right) * \frac{2 * U_0}{G_F * U_I}$$

The above equation converted the raw data into the stress profile in the sample. Divided by the modulus of the specimen, the stress profile was further converted to the strain profile in the specimen. From here the wave form transmitted into the specimen looks like Fig 4.17.

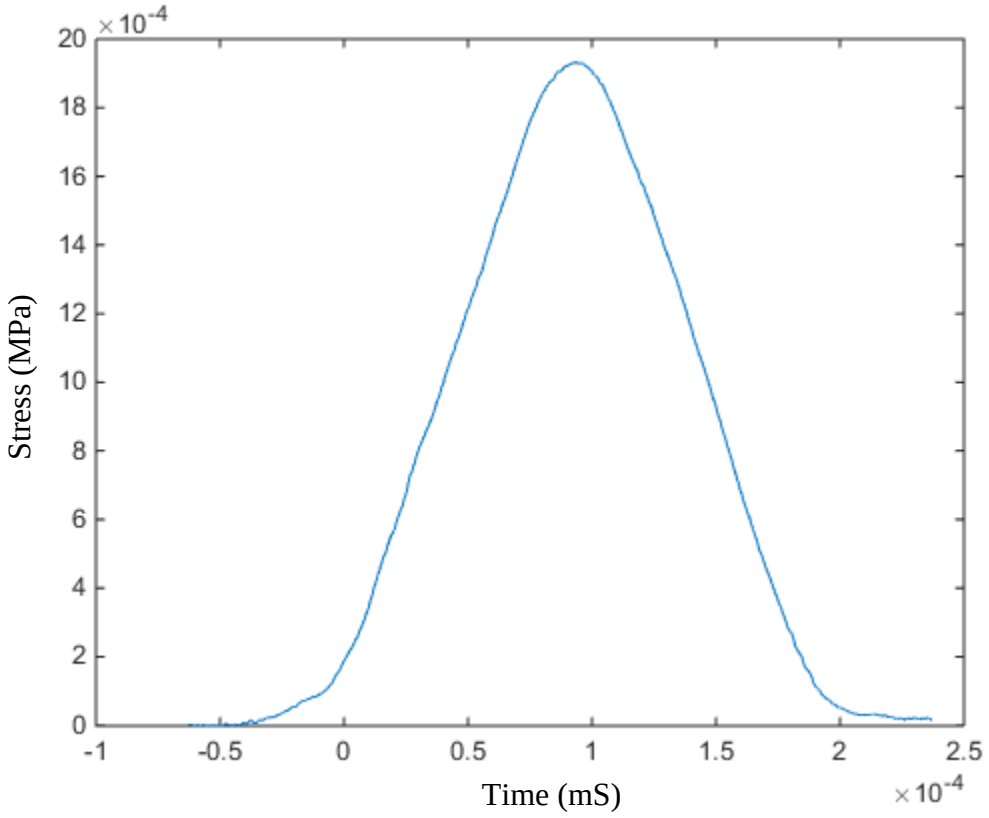

Figure 0.17 Stress transmitted into sample

The next step in the analysis was to create an inverse of the transmitted wave to model the wave being reflected back from the free end. As the wave is reflected back, the strain in the specimen is equivalent to the sum of the reflected and transmitted waves. Due to creating a reflected wave via software analysis, the resultant graph (Fig 4.18) shows a combined waveform where the entire left side of the graph is imaginary. In the figure below it can be seen from the

wave overlapping results that the specimen (at the moment in time that this graph represents) is primarily under a constant compressive strain rate.

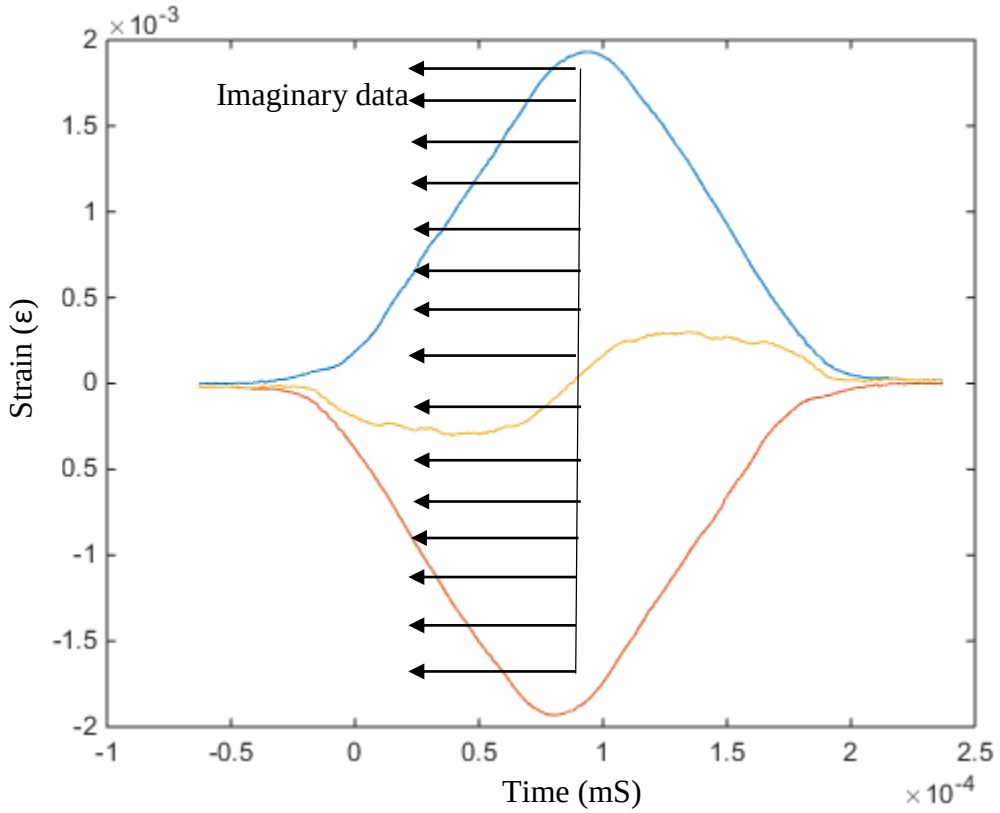

Figure 0.18 Strain rate profile of specimen

By shifting the two data columns in opposite directions, a model is created of how the strain (and stress) in the sample changes as the wave is reflected back in tension. In the time column, the data is shifted up, and in the compression column the data is shifted down. Making shifts of only one row represents a shift in time of two microseconds. As time progresses, the stress remains constant while moving into tension (see Fig 4.19).

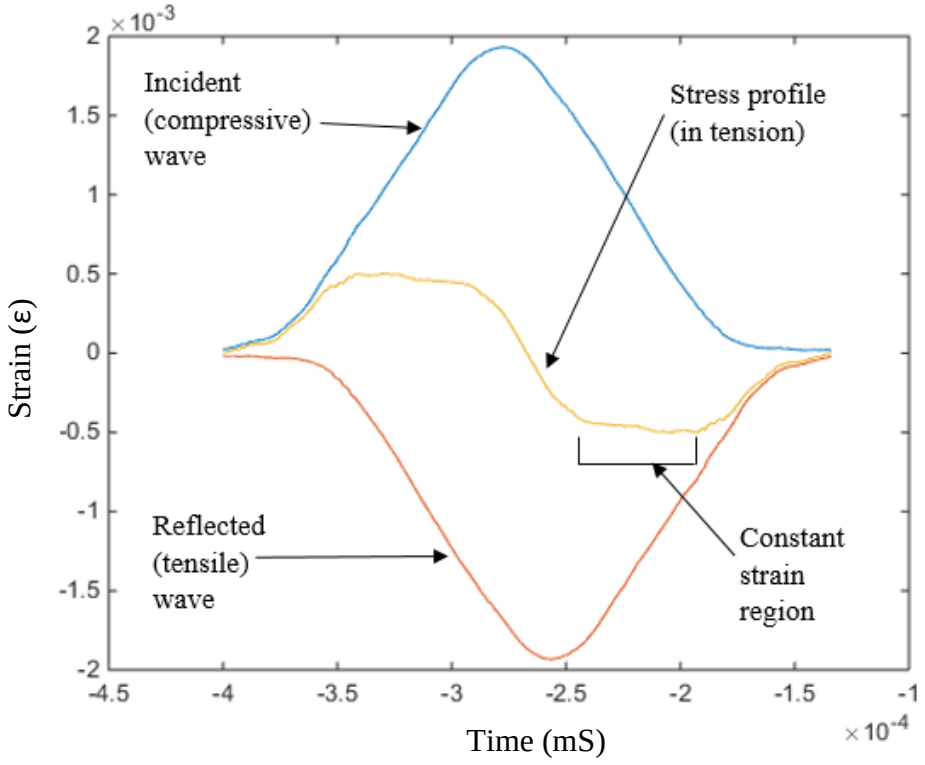

Figure 0.19 Summation of compression and reflected waves now in tension

As the columns were being shifted to represent a progression in time, the values of strain were carefully monitored. Beginning when the strain was (approximately) zero, the strain value for each shift was calculated. This was achieved by converting the spall distance into time (using the wave speed of the material), and the corresponding strain was recorded. This value gave the strain of the material at the spall location for a particular point in time.

The recorded strain value was converted to stress and was also recorded. This was repeated until the stress value reached the spall strength (averaging about 100 iterations per sample). Once the spall strength value was reached, the strain data was plotted against the relevant time intervals. Taking the slope of this relationship determines the strain rate that was present at the

moment of failure. A Matlab code to perform all these functions for subsequent calculations was constructed (see Appendix A).

CHAPTER 5

CONCLUSION

Experiments were carried out to determine the feasibility of a new technique that would satisfy the boundary conditions required for determining the dynamic tensile strength of brittle heterogeneous materials. Furthermore, two techniques for the analysis of the experimental results were explored.

It was proven both theoretically and experimentally that a loading wave on a modified Kolsky bar setup could be tailored, by the use of pulse shaping, to achieve a linear, symmetrical shape (isosceles triangle shape). Achieving this shape was shown to satisfy experimental boundary conditions (stress equilibrium and constant strain rate) that were the source of much debate in prior experiments. Achieving these boundary conditions shows great promise for the future of spall testing.

A laser extensometer was used to analyze the spall strength of a specimen. Upon examination of this technique, it was determined that taking a time derivative to determine the spall velocity introduced an indeterminable amount of noise, and was thus believed to be insufficient for analysis of the spall event.

Digital Image Correlation was used as an alternative technique to analyze spall velocity and strain during the event. For determining the spall velocity, the DIC technique tracked displacement and then used a time derivative to calculate velocity. Like the laser extensometer, this was determined to be insufficient due to the small deformation of the specimen. For determining the strain, the DIC tracks speckle patterns on the specimen and then uses the change in distance between the speckles to calculate strain. The concrete was determined to fail at a tensile strain of approximately 0.0002. This small strain was proved to be too small to be

accurately captured by the cameras, which resulted in inconsistent results. The DIC was then determined to be insufficient for analysis of the spall technique.

Future Work

Further work is needed in the area of analysis of the spall event. Furthermore, this project only analyzed one strain rate at which to fail the concrete. More pulse shaping and experimentation will be required to achieve more valid loading waves at different strain rates.

A laser vibrometer is a device that measures velocity directly (without taking a time derivative). This device will be a logical next step in determining a suitable analysis technique.

APPENDIX A: MATLAB CODE FOR BATCH PROCESSING

```
%% define constants
clear;
clc;
Vin=15;
Gain=100;
Eb=200; % bar modulus in Gpa
Ec=45.5; % concrete modulus in Gpa
Cb=5000; % wave speed in bar
Cc=4550; % wave speed in sample (m/s)
SpallDistance=.085;%Distance (m) from spall end to first crack
Gauge=2.08;
PulseWidth=1500;% pulse duration (# of points)
Spallstrength=10;


%% import data
uiimport;

%%
t=Time;
strain=Ampl-mean(Ampl(1:1000)); % shift base line to zero
thresh=0.2;


for i=1:length(strain)
    if strain(i)>thresh
       start=i;

       break
    end
end

start=start-350;
Ipulse=strain(start:start+PulseWidth);
tpulse=t(start:start+PulseWidth);
plot(tpulse,Ipulse)
%%

Rpulse=-flipud(Ipulse);% create reflected pulse by flipping incindent pulse
Spulse=Ipulse+Rpulse;

plot(tpulse,Ipulse,tpulse,Rpulse,tpulse,Spulse)
%% find "y=0"

N=200; % number of iterations to search for "y=0"
Devi=zeros(N,1); % initialize array to store standard deviation at each point

for i=1:N

I=Ipulse(i+1:length(Ipulse));% shift incident pulse right
R=Rpulse(1:length(Rpulse)-i); % shift reflected pulse left
S=(I+R); % calculate stress profile
```

```
tpulse=t(1:length(Ipulse)-i);

Devi(i)=std(S);
plot(tpulse,I,tpulse,R,tpulse,S)

 pause(0.05)

end
index=0;
%%

FracTime=SpallDistance/Cc;%Distance to crack in seconds
spallcount=round(FracTime/(t(2)-t(1)));

%%

z=1;%initialize counter
Strainplot=zeros(z,1);%Start array to plot strain rate
Stressplot=zeros(z,1);%Start array to plot stress

while z<150
[devi,index]=min(Devi); %index where stress is "zero"
index=index+67+z; % step forward in time a bit


I=Ipulse(index+1:length(Ipulse));% shift incident pulse right
R=Rpulse(1:length(Rpulse)-index); % shift reflected pulse left
S=(I+R);% calculate stress profile

[minimum,izero]=min(abs(S(1:length(S))));% find where stress crosses x axis


if izero>150;
    yzero=izero+49;
else
    izero=izero+1;
end

index=0;


CrackLoc=yzero+spallcount;




Crackvolt=abs(S(CrackLoc));

BStrain=(2*Crackvolt)/(Gain*Vin*Gauge);

CrackStress_MPa=BStrain*Ec*10^3;
```

```
Stressplot(z)=CrackStress_MPa;
Strainplot(z)=BStrain;
z=z+1;

end

%%
timerate=[0:(1*10^-7):(1*10^-7)*(length(Strainplot)-1)];

plot(timerate,Strainplot)

polyfit(timerate,Strainplot,1)
```

APPENDIX B: ADAPTER CAD DRAWING

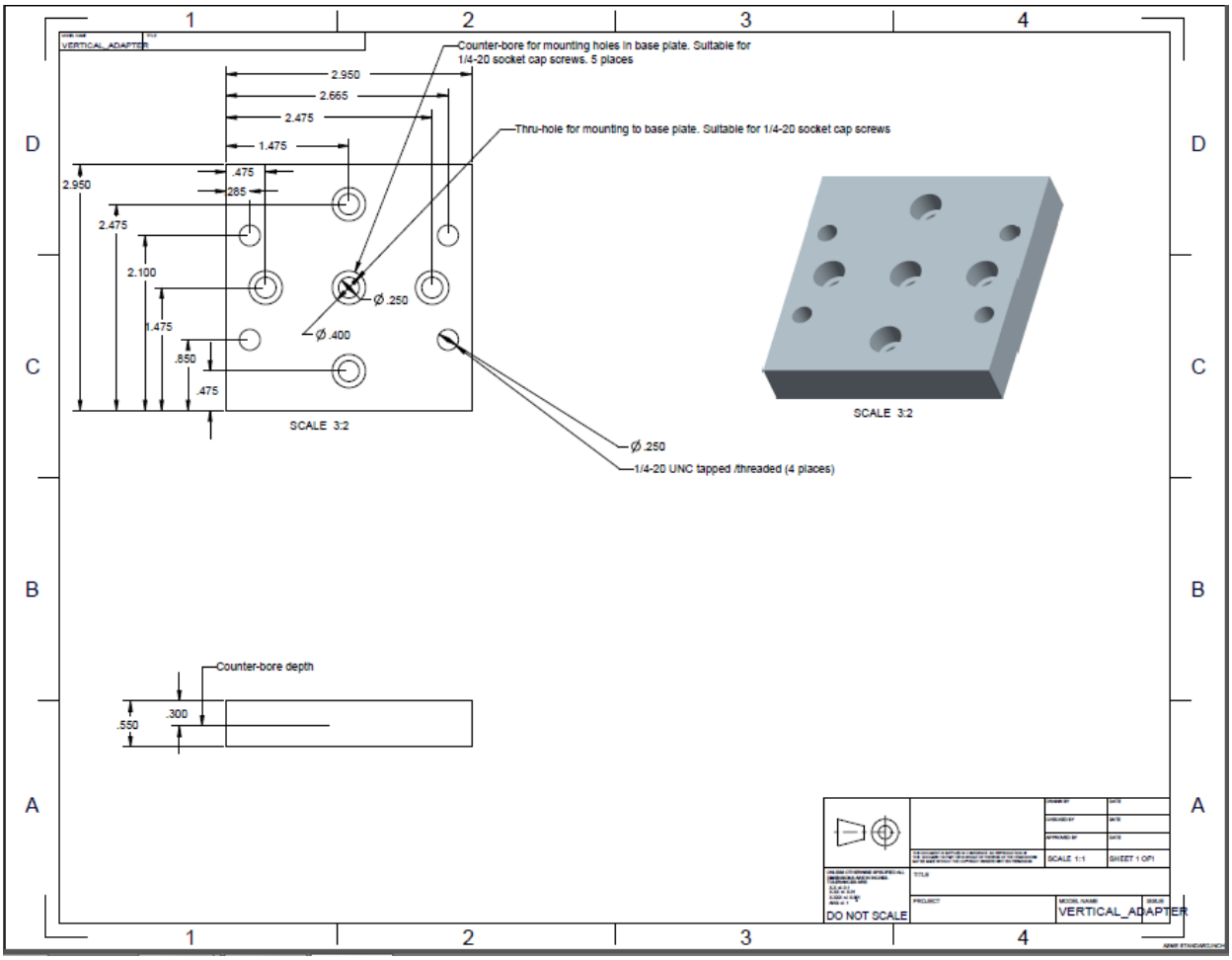

REFERENCES

[1] W. Chen, B. Song, “Split Hopkinson (Kolsky) Bar: Design, Testing and Applications”, Springer, 2011

[2] Song, B., Chen, W.: Loading and unloading split Hopkinson pressure bar

pulse-shaping techniques for dynamic hysteretic loops. Exp. Mech. 44, 622-627 (2004c)

[3] Cheng, M., Chen, W., Weerasooriya, T.: Mechanical behavior of bovine

tendon with stress-softening and loading rate effects. Adv. Theory of Appl. Mech. 2, 59-74 (2009)

[4] Y.B. Lu, Q.M. Li: About the Dynamic Uniaxial Tensile Strength of Concrete-Like Materials. International Journal of Impact Engineering. Vol 38, 4, 171-180 (2011)

[5] F. Galvez Diaz-Rubio, J. Rodriguez Perez, V. Sanchez Galvez: The Spalling of Long Bars as a Reliable Method of Measuring the Dynamic Tensile Strength of Ceramics. International Journal of Impact Engineering. Vol 27, 2, 161-177 (2002)

[6] Dean, A.W., Heard, W. F., Loeffler, C. M., Martin, B. E., Nie, X.: A New Theory for Kolsky Bar Dynamic Spall Tests. Journal of Dynamic Behavior of Materials, Vol, (2016)

[7] M. Meyers, “Dynamic Behavior of Materials”, John Wiley & Sons, Inc., 1999